THE ASTROPHYSICAL JOURNAL SUPPLEMENT SERIES, 131:441–463, 2000 December

COMPARING GALAXY MORPHOLOGY AT ULTRAVIOLET AND OPTICAL WAVELENGTHS

L. E. KUCHINSKI,[1] W. L. FREEDMAN,[2] BARRY F. MADORE,[1,2] M. TREWHELLA,[1] R. C. BOHLIN,[3] R. H. CORNETT,[4] M. N. FANELLI,[4,5] P. M. MARCUM,[6] S. G. NEFF,[7] R. W. O'CONNELL,[8] M. S. ROBERTS,[9] A. M. SMITH,[7] T. P. STECHER,[7] AND W. H. WALLER[4,10]

Received 1999 December 18; accepted 2000 February 9

ABSTRACT

We have undertaken an imaging survey of 34 nearby galaxies in far-ultraviolet (FUV, ~1500 Å) and optical (*UBVRI*) passbands to characterize galaxy morphology as a function of wavelength. This sample, which includes a range of classical Hubble types from elliptical to irregular, with emphasis on spirals at low inclination angle, provides a valuable database for comparison with images of high-z galaxies whose FUV light is redshifted into the optical and near-infrared bands. Ultraviolet data are from the Ultraviolet Imaging Telescope (UIT) Astro-2 mission. We present images and surface brightness profiles for each galaxy, and we discuss the wavelength dependence of morphology for different Hubble types in the context of understanding high-z objects. In general, the dominance of young stars in the FUV produces the patchy appearance of a morphological type later than that inferred from optical images. Prominent rings and circumnuclear star formation regions are clearly evident in FUV images of spirals, while bulges, bars, and old, red stellar disks are faint to invisible at these short wavelengths. However, the magnitude of the change in apparent morphology ranges from dramatic in early-type spirals with prominent optical bulges to slight in late-type spirals and irregulars, in which young stars dominate both the UV and optical emission. Starburst galaxies with centrally concentrated, symmetric bursts display an apparent "E/S0" structure in the FUV, while starbursts associated with rings or mergers produce a peculiar morphology. We briefly discuss the inadequacy of the optically defined Hubble sequence in describing FUV galaxy images and estimating morphological k-corrections, and we suggest some directions for future research with this data set.

Subject headings: galaxies: structure — ultraviolet: galaxies

1. INTRODUCTION

An understanding of the ultraviolet (UV) properties of local galaxies is essential for interpreting images of high-redshift systems and especially critical in searches for morphological evolution in the galaxy population. At redshifts of $z \sim 3$–10, the rest-frame UV light of galaxies is shifted into the optical (1500 Å observed in the V band at $z \sim 2.7$) and near-infrared (1500 Å observed in the H band at $z \sim 10$) regions of the spectrum that are easily observable from the ground. Although one operational approach to overcoming this "band-shifting" problem is to observe in the infrared (e.g., Teplitz et al. 1998), the rate of data acquisition for galaxy images is generally highest at optical wavelengths, where detectors are larger and the sky background is lower than in the infrared. Under these circumstances, the most direct method for comparing present-day galaxies to those in the early universe is to build a large sample of local UV galaxy data.

Recent deep surveys suggest that galaxies with peculiar morphology are more prevalent at high redshift (e.g., Brinchmann et al. 1998; Abraham et al. 1996). However, it is difficult to quantify the influence of band-shifting on observed differences between the optical characteristics of nearby galaxies and the rest-frame UV appearance of distant ones because UV and optical morphology are not often well-coupled (O'Connell 1997a; Marcum et al. 1997; P. M. Marcum et al., in preparation). Rest-frame UV images of galaxies often suggest a later Hubble type than the corresponding optical appearance: bulges are less prominent, galaxy light appears more patchy, and in extreme cases the different star-forming regions in a single galaxy may appear as separate systems in the UV (O'Connell 1997a; O'Connell & Marcum 1996). On the other hand, recent deep NICMOS imaging of distant galaxies at longer rest wavelengths suggests that some of the morphological peculiarities are still visible in the optical and thus are intrinsic in the galaxies' structure (e.g., Bunker 1999; Teplitz et al. 1998). Although methods exist to estimate UV morphology by extrapolation from optical data (Abraham 1998; Abraham, Freedman, & Madore 1997), they rely on the use of global galaxy spectral energy distributions that may not accurately represent localized conditions, especially in dusty or starbursting regions. For example, Donas, Milliard, & Laget (1995) find a variation among $UV-b$ colors in galaxies with identical $b-r$. The availability of far-ultraviolet (FUV) images for bright, well-resolved galaxies of a range of Hubble types would facilitate a more direct comparison between local and distant galaxy populations.

[1] Infrared Processing and Analysis Center, Caltech/Jet Propulsion Laboratory, Pasadena, CA 91125.
[2] Observatories of the Carnegie Institution of Washington, Pasadena, CA 91101.
[3] Space Telescope Science Institute, Baltimore, MD 21218.
[4] Raytheon ITSS Corp., NASA Goddard Space Flight Center, Greenbelt, MD 20771.
[5] Department of Physics, University of North Texas, Denton, TX 76023.
[6] Department of Physics, Texas Christian University, Fort Worth, TX 76129.
[7] Laboratory for Astronomy and Solar Physics, NASA Goddard Space Flight Center, Greenbelt, MD 20771.
[8] Department of Astronomy, University of Virginia, Charlottesville, VA 22903.
[9] National Radio Astronomy Observatory, Charlottesville, VA 22903.
[10] Department of Physics and Astronomy, Tufts University, Medford, MA 02155.

The appearance of galaxies in the UV is determined primarily by emission from hot stars and by the distribution of dust, with a contribution in the central regions from an active galactic nucleus (AGN) if one is present and unobscured. Light in the $\sim$1500 Å far-ultraviolet (FUV) band of the Ultraviolet Imaging Telescope (UIT; Stecher et al. 1997) originates in young objects of spectral types O and B (Fanelli et al. 1997a) and, if old populations are present, in certain types of low-mass stars in late stages of evolution (the "UVX" population; see O'Connell 1999 for a review). Thus, this region of the spectrum can probe timescales of young stellar populations between that studied via Hα emission (only O stars, $\sim$5 Myr) and that evident in the optical colors (which trace the age of a stellar population on timescales of a few Gyr; O'Connell 1997b).

Opacity due to dust in the FUV is a factor of $\sim$2.5 higher than in the optical V band, assuming a Galactic extinction law (Cardelli, Clayton, & Mathis 1989), and even larger for Small Magellanic Cloud–type dust (Gordon, Calzetti, & Witt 1997). The young, massive stars that provide the bulk of the UV emission also tend to have small scale heights, less than or similar to that of the dust, while older stars that dominate at optical wavelengths and have scale heights greater than that of the dust layer (Mihalas & Binney 1981). The degree to which dust extinguishes the UV light of highly inclined disk galaxies is unclear. It likely depends strongly on the relative geometry of star-forming regions and dust concentrations, a phenomenon recently noted in optical/NIR studies of nearby galaxies as well as in theoretical studies of systems with a mixture of stars and dust (Kuchinski et al. 1998; Gordon et al. 1997; Huizinga 1995). For instance, NGC 4631 is quite bright in the FUV and blue in FUV–optical colors, and it does not show evidence of strong attenuation (Smith et al. 1997, 2000; O'Connell 1997a). However, NGC 891 is only barely detected (Marcum et al. 1997; P. M. Marcum et al., in preparation), a phenomenon that Smith et al. suggest is due to extinction effects. UV morphology may also be dramatically influenced by specific features such as dust lanes, as noted in Cen A by O'Connell (1997a). Scattering by dust grains is quite efficient in the FUV (Witt et al. 1992) and may contribute significantly to the emission near H II regions and in spiral arms (Waller et al. 1997a; Stecher et al. 1982).

Prior to the Space Shuttle–borne UIT Astro missions, UV imaging of galaxies was limited to low resolution and/or small fields of view (see Brosch 1999 for a detailed review). UIT-prototype rocket-borne experiments in the 1980s provided images of five nearby galaxies with a resolution of $\sim$15″ and 10 more with a resolution of 100″ (Hill, Bohlin, & Stecher 1984; Bohlin et al. 1991). The FOCA balloon experiment yielded images of similar resolution for six nearby galaxies (Blecha et al. 1990). Recently, higher resolution UV images of 110 galaxy nuclei (Maoz et al. 1996) and nine starburst galaxies (Meurer et al. 1995) have been obtained at 2200 Å using the *Hubble Space Telescope* (*HST*) Faint Object Camera with a very small (22″) field of view. A FUV ($\sim$1500 Å) survey of galaxies at redshifts of $\sim$0.1–0.2 is also underway using the Space Telescope Imaging Spectrograph, again with a small (25″) field of view (Gardner et al. 1997). With a 40′ field of view and $\sim$3″ resolution, UIT was optimally suited to study the morphology of nearby galaxies with good resolution. The usefulness of UV and optical images and radial profiles to study morphology variations with wavelength was demonstrated by Cornett et al. (1994) with UIT Astro-1 data for M74, by Hill et al. (1997) for M51, and by Reichen et al. (1994) for M81.

In this and a companion paper (P. M. Marcum et al., in preparation), we present the results of a UV–optical imaging survey of nearby bright galaxies. The UV images were obtained by the UIT during the Astro-1 and Astro-2 *Spacelab* missions in 1990 and 1995, respectively. Ground-based optical CCD images of the sample galaxies were obtained with pixel scales and fields of view approximately comparable to those of the UIT images. The Astro-1 data presented in Marcum et al. include both FUV ($\sim$1500 Å) and near-ultraviolet (NUV; $\sim$2500 Å) data as well as optical images for 43 galaxies. This paper includes FUV and optical data for 34 galaxies observed during Astro-2 with Hubble types specifically chosen to span the range E to Irr, including some interacting/merging systems. There is some emphasis in the sample selection on face-on spirals in which spiral arm, bar, and ring morphologies are easily observed. In § 2 we discuss the sample selection, describe the UIT and optical observations, and explain the basic data reduction. Section 3 contains details of the registration of FUV and optical images and the extraction of surface brightness and color profiles. A qualitative comparison of UV and optical morphology, based on the images and profiles, is presented in § 4. In § 5 we provide a brief summary and discuss avenues of future investigation, including studies of the morphological k-correction and analysis of the star-formation histories of individual galaxies. In a subsequent paper (Kuchinski et al. 2000), we will investigate the quantitative concentration and asymmetry indices for these galaxies and consider the implications of these results for the study of high-redshift galaxies.

2. OBSERVATIONS AND DATA REDUCTION

2.1. *Sample Selection*

Our sample consists of 34 galaxies observed with UIT during the Astro-2 mission, for which we have also obtained ground-based optical images. Many of the galaxies were selected as part of a UIT Guest Observer program specifically to investigate the UV morphology in prototypes of different Hubble types. Others were observed during UIT studies of starburst galaxies (e.g., Smith et al. 1996), early-type galaxies (Ohl et al. 1998), AGNs (Fanelli et al. 1997a), or individually for selected purposes. It is important to remember that while this sample does contain galaxies with a range of morphologies, it was not chosen to statistically represent the relative distribution of Hubble types in the local population. The galaxies have types E to Irr ($T = -5.0$ to $+10.0$), and are located at distances of $\sim$2–25 Mpc ($H_0 = 75$ km s^{-1} Mpc^{-1}). Late-type systems in which star formation produces prominent morphological features in the FUV are emphasized. Three sets of interacting pairs are included: NGC 3226/3227, NGC 4038/4039, and NGC 5194/5195. Table 1 gives basic properties of the sample galaxies.

2.2. *Ultraviolet Observations and Data Reduction*

The sample galaxies were observed in the FUV with UIT, a 38 cm Ritchey-Chretien telescope mounted on the Astro payload. The Astro-2 mission, during which these data were obtained, was flown on the space shuttle *Endeavour* on 1995 March 2–18. Details of the telescope and instrumentation,

as well as specific information about pipeline data processing of the UV images, can be found in Stecher et al. (1997) and will be briefly summarized here. Only the FUV ($\sim$1500 Å) camera was operational during the Astro-2 mission. Two FUV filters were used: the B1 filter with an effective wavelength of 1520 Å and width 354 Å, and the slightly narrower B5 filter with effective wavelength of 1615 Å and width 225 Å, which was used during daylight observations to exclude dayglow emission lines (Hill et al. 1998; Waller et al. 1995). Based on observations of early-type galaxies (Ohl et al. 1998), there is no evidence for a "red leak" in the system. The camera consisted of a two-stage image intensifier coupled to Kodak IIa-0 film, on which the images were recorded. The photographic film was digitized with a 20 μm square aperture and 10 μm sample spacing, then binned to a 20 μm spacing (Stecher et al. 1997). In the pipeline data reductions, background "fog" from the photographic film was subtracted, and the images were linearized, flat-fielded, and calibrated. The final output images have a scale of 1.″136 per pixel and a typical point-spread function (PSF) of FWHM $\sim$ 3″ in the central 16′ of the frame, in which nearly all the galaxies studied here are imaged (Stecher et al. 1997). UIT images with enough stars to calculate astrometric solutions were corrected for distortion (Stecher et al. 1997; Greason et al. 1994); these data products were used where available. However, we note that even on uncorrected images, the uncertainty due to distortion in the central part of the frame (where most of our galaxy images are located) is less than or equal to the PSF FWHM.

After visual inspection of all available FUV images for each galaxy, we selected the ones with the best signal-to-noise ratio and image quality for further analysis. In most cases this is the image with the longest exposure time, unless that image is noted in the UIT log as suffering pointing problems or other defects. In such cases, the longest exposure time image of good quality was used. The UV-bright center of NGC 4151 is saturated in the UIT Astro-2 images; for photometry of this galaxy, see Fanelli et al. (1997a). We select a long-exposure UIT image of this galaxy to show the faint spiral arms as well as the active nucleus. The UIT exposure time of the image selected for each galaxy is given in Table 2.

Many of the FUV images required no further processing beyond the UIT pipeline, but some have a noticeable "stripe" artifact through the center of the frame (Stecher et al. 1997). If the entire galaxy was located within the stripe, no correction was made, and care was taken to determine the sky value within the stripe as well. For galaxies located partly within and partly outside the stripe, a quadratic surface was fitted to the frame after masking out the central region (where the galaxy lies) and the frame edges. This surface was then subtracted before the sky background and surface brightness profile were measured. The FUV sky background is typically low (see Waller et al. 1995 for a discussion of the UV background), ranging from undetectable (with a 1 σ limit of $\sim$25 mag arcsec^{-2}) up to 22 mag arcsec^{-2} for a few images acquired during daylight.

2.3. *Optical Observations and Data Reduction*

Broadband optical images of the sample galaxies were obtained over the past several years with the Las Campanas Observatory 2.5 m du Pont telescope, the CTIO 1.5 m telescope, and the Palomar 1.5 m and 5 m telescopes. All the galaxies presented here were imaged in at least one of the $UBVR_CI_C$ bands; many have multicolor photometry. Observations at Las Campanas were carried out using the 2048 $\times$ 2048 Tek 5 CCD with a scale of 0.″26 per pixel. The CTIO observations utilized the Tek 2048 $\times$ 2048 CCD with a scale of 0.″43 per pixel. Data from the Palomar 1.5 m telescope were taken using the 2048 $\times$ 2048 CCD13 or CCD16 with a scale of 0.″37 per pixel; some of these were binned to 1024 $\times$ 1024 with a scale of 0.″74 per pixel. Observations with the Palomar 5 m telescope used the COSMIC camera with a 2048 $\times$ 2048 CCD and a scale of 0.″28 per pixel; again, some images were binned to a scale of 0.″55 per pixel. Table 2 shows the telescope, filters, and exposure times for each galaxy.

Data reduction for the optical images was carried out using the IRAF (Tody 1986) and VISTA (Stover 1988) packages. The images were bias-subtracted and flat-fielded with twilight or dome flats for each filter. An apparent gradient in the background of some of the V, R, and I frames taken at Palomar remained after these steps. A planar surface was fitted to these frames after masking out the galaxy, then subtracted before further processing. Cosmic rays were identified with the IRAF "*cosmicrays*" package and were replaced with an average of surrounding pixel values. If more than one data frame was available for a galaxy in a specific filter, the frames were registered using the coordinates of several bright stars, scaled to the same exposure time, and a zero-point offset was applied to match the background levels. The frames were then averaged (for two) or median combined (for three or more). Some of the images are saturated at the galaxy centers; no correction is applied, but the saturated pixels were flagged for future consideration. Sky levels were determined in boxes away from the galaxy. In some cases (flagged in Table 2) the galaxy nearly fills the frame, and thus the background level is somewhat uncertain. On images in which several regions of sky away from the galaxy can be measured, the typical rms scatter in sky levels across the frame is less than 2% of the sky value.

2.4. *Data Calibration*

Calibrations were applied to each image to obtain the approximate relative alignment of the multicolor light profiles presented in § 3. The UIT data were calibrated using standard stars measured by the *International Ultraviolet Explorer* (*IUE*). The resulting flux calibration is estimated to be accurate to $\sim$15% (Stecher et al. 1997); this value includes the uncertainty in the final *IUE* calibration. Magnitudes are on the monochromatic system:

$$\mathrm{mag}_\lambda = -2.5\log_{10}(f_\lambda) - 21.1\ , \qquad (1)$$

where the flux is in units of ergs cm^{-2} s^{-1} Å^{-1}. Calibration data for each image are stored in the image headers of the UIT data products.

Because many of the optical data were obtained under nonphotometric conditions, the frames were calibrated via comparison to published aperture photometry for each galaxy. We used the catalog of Prugniel & Heraudeau (1998), excluding any data whose zero point was found by these authors to be systematically offset by more than 0.05 mag from that galaxy's curve of growth. We calculated the difference between a synthetic aperture magnitude measured on our galaxy image and the published value for each of the tabulated apertures that fit on our frame. After

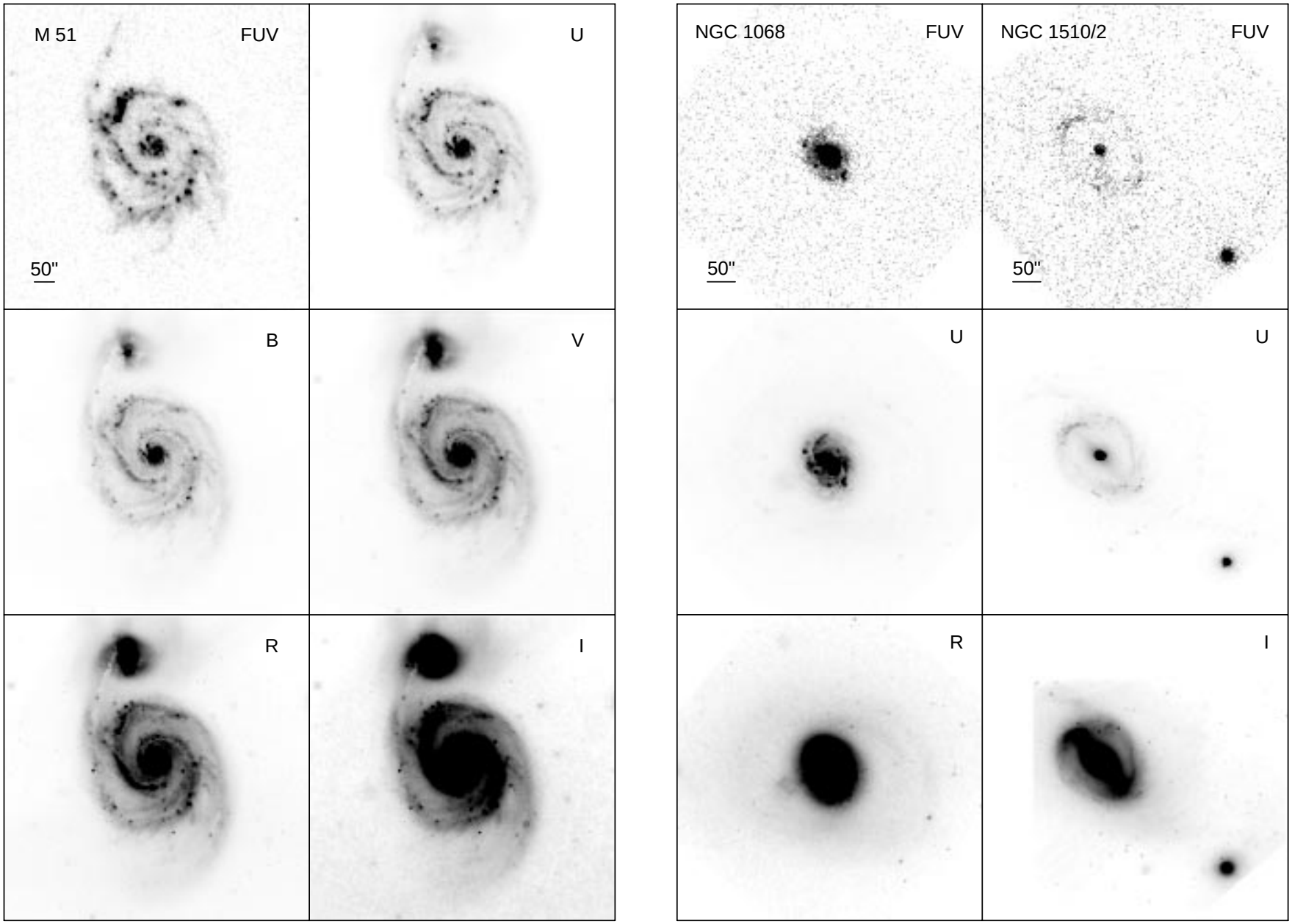

FIG. 1.—FUV and optical images of sample galaxies. All images are registered to the FUV coordinate system and oriented with north up and east to the left. As noted in the text, the images are displayed such that pixels of the same brightness (flux) have constant gray level for all images of the same galaxy. Scale bars, which are relevant to all images of a particular galaxy, are shown on each of the FUV panels.

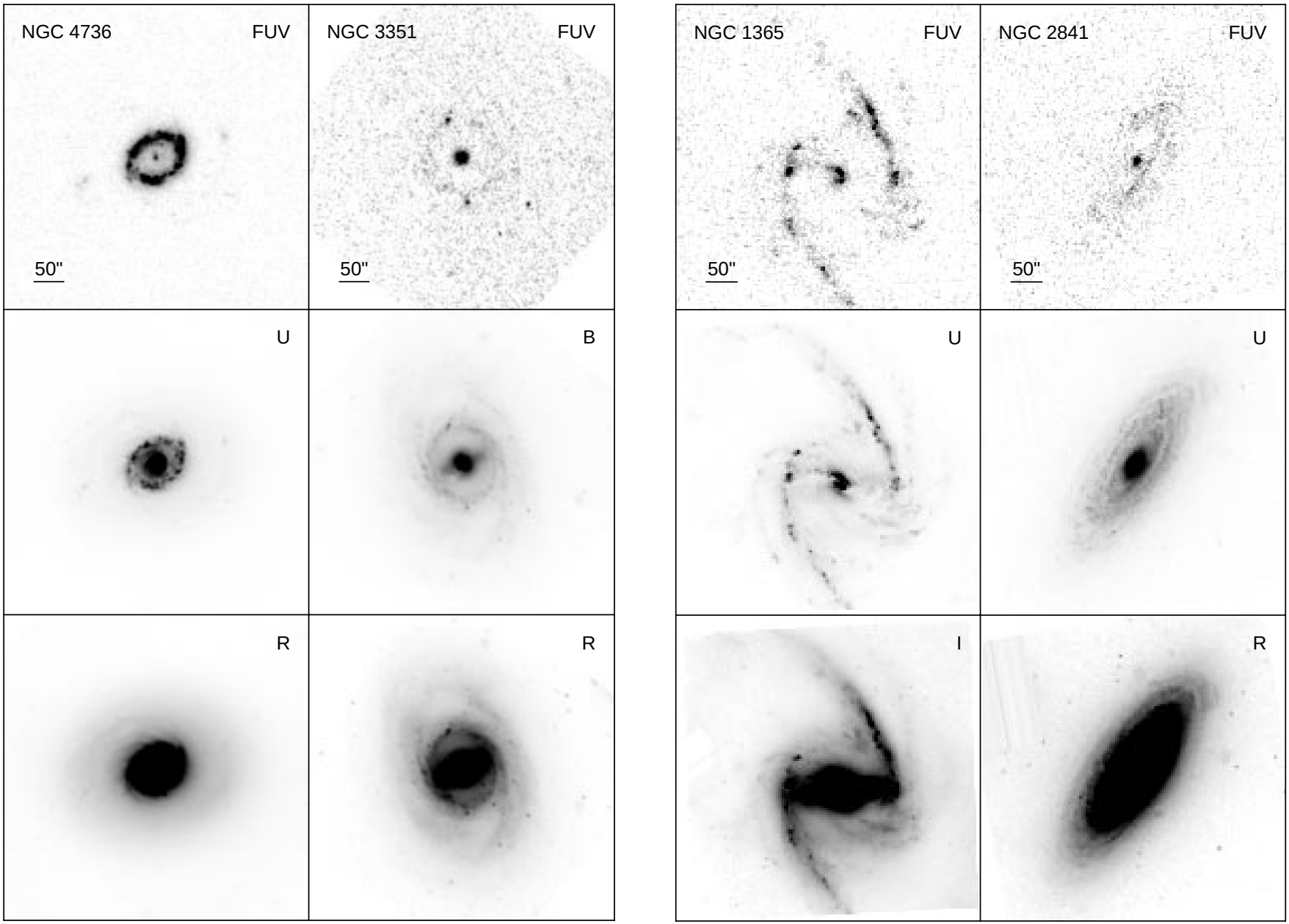

FIG. 1.—*Continued*

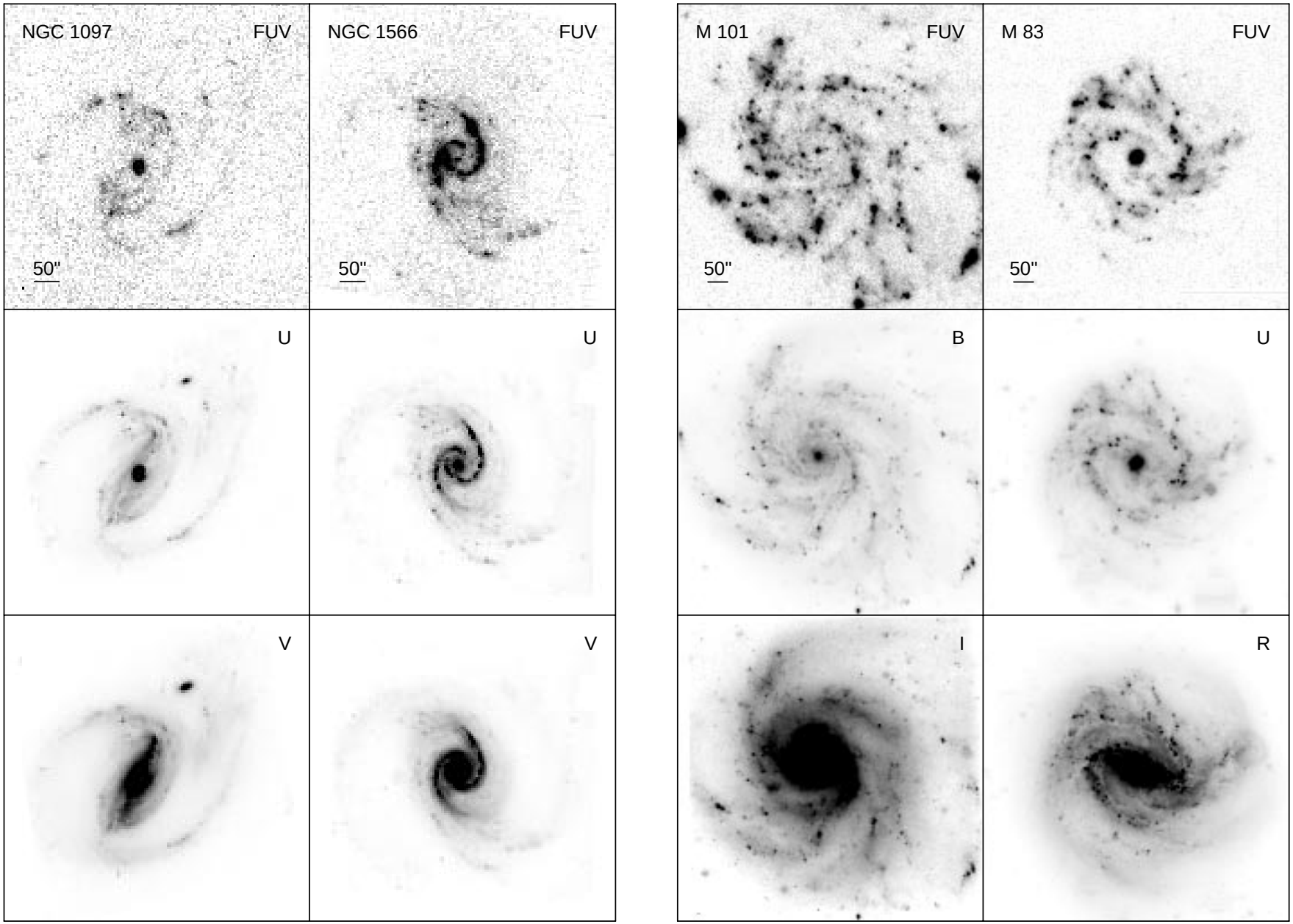

FIG. 1.—*Continued*

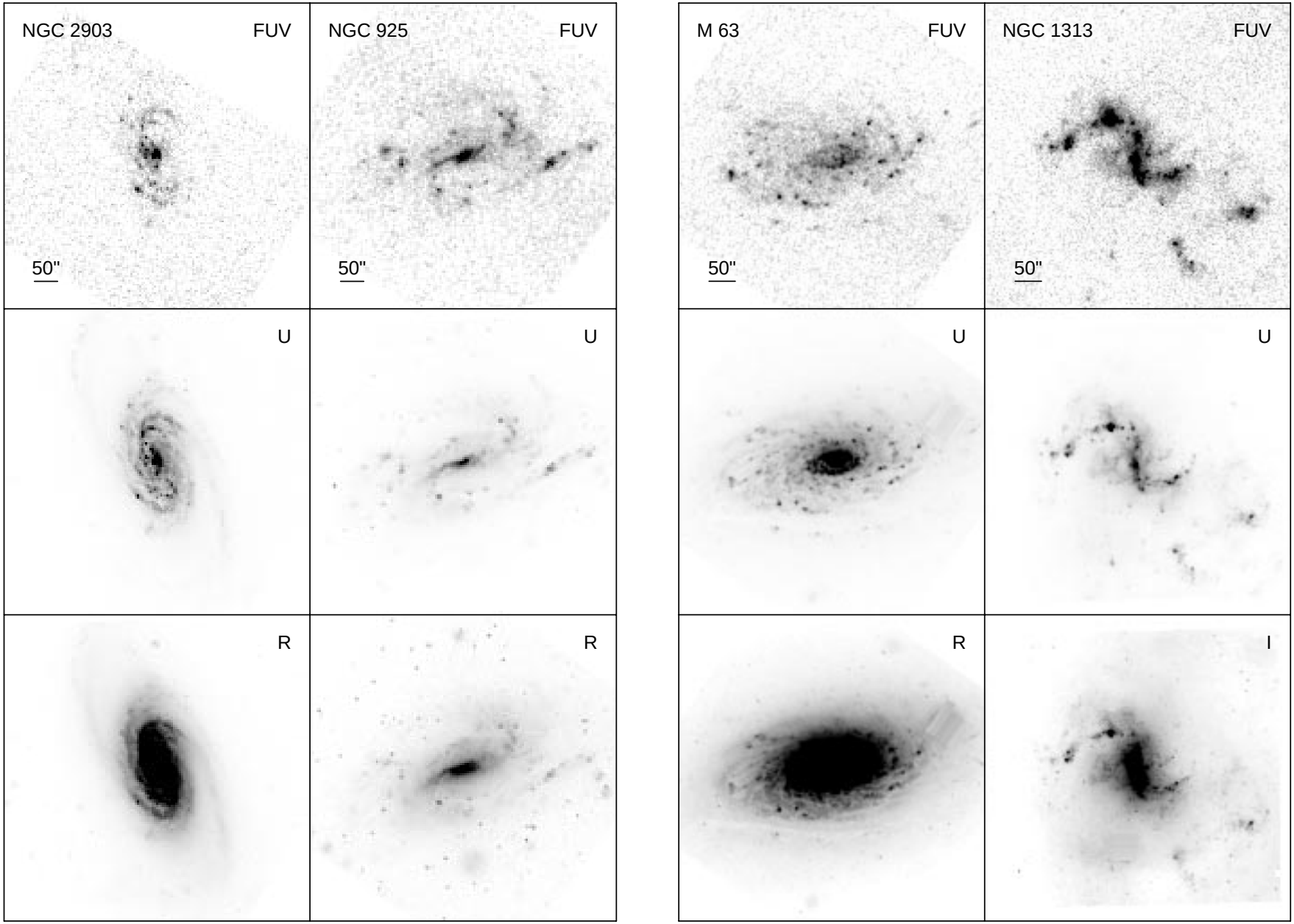

FIG. 1.—*Continued*

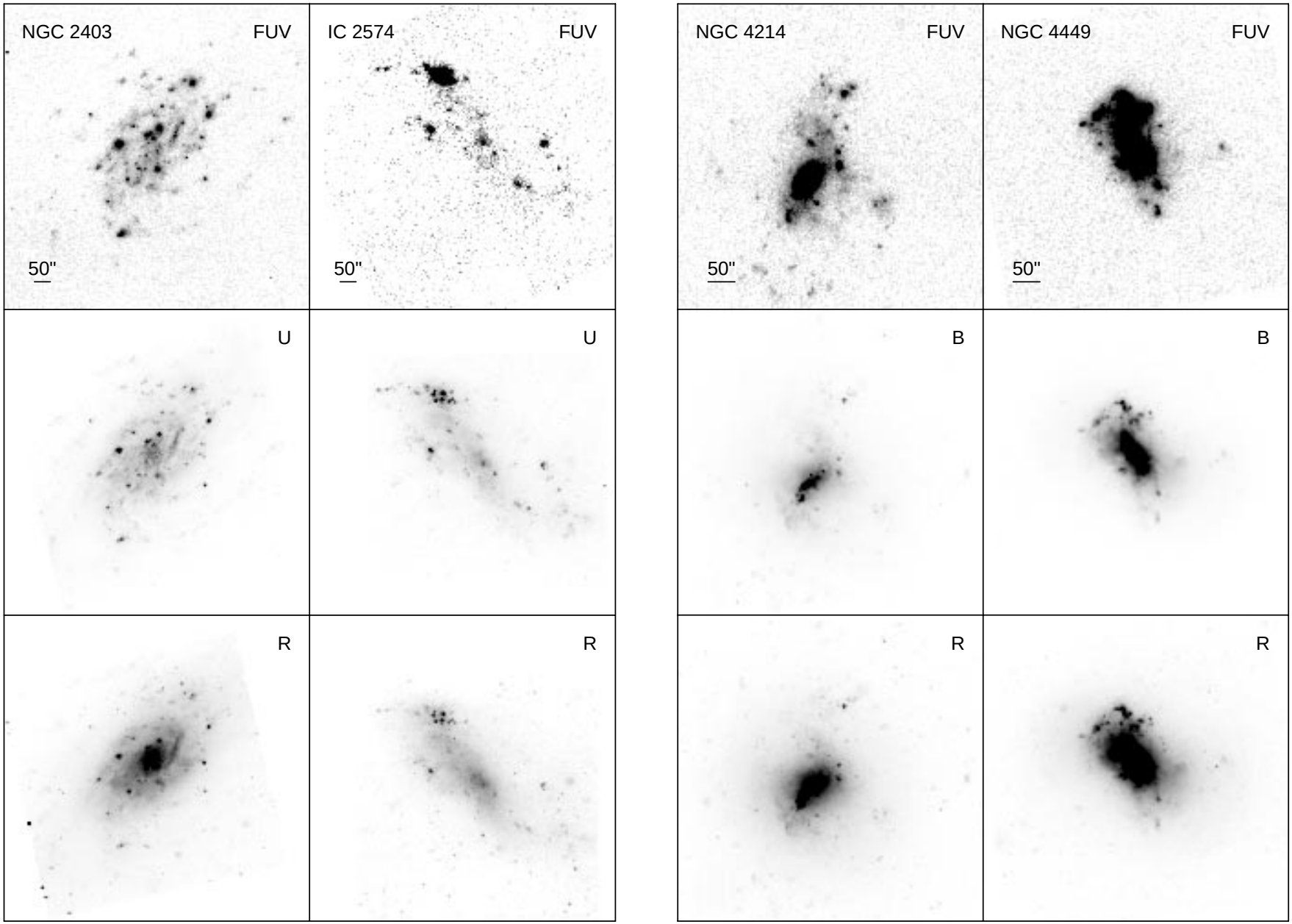

FIG. 1.—*Continued*

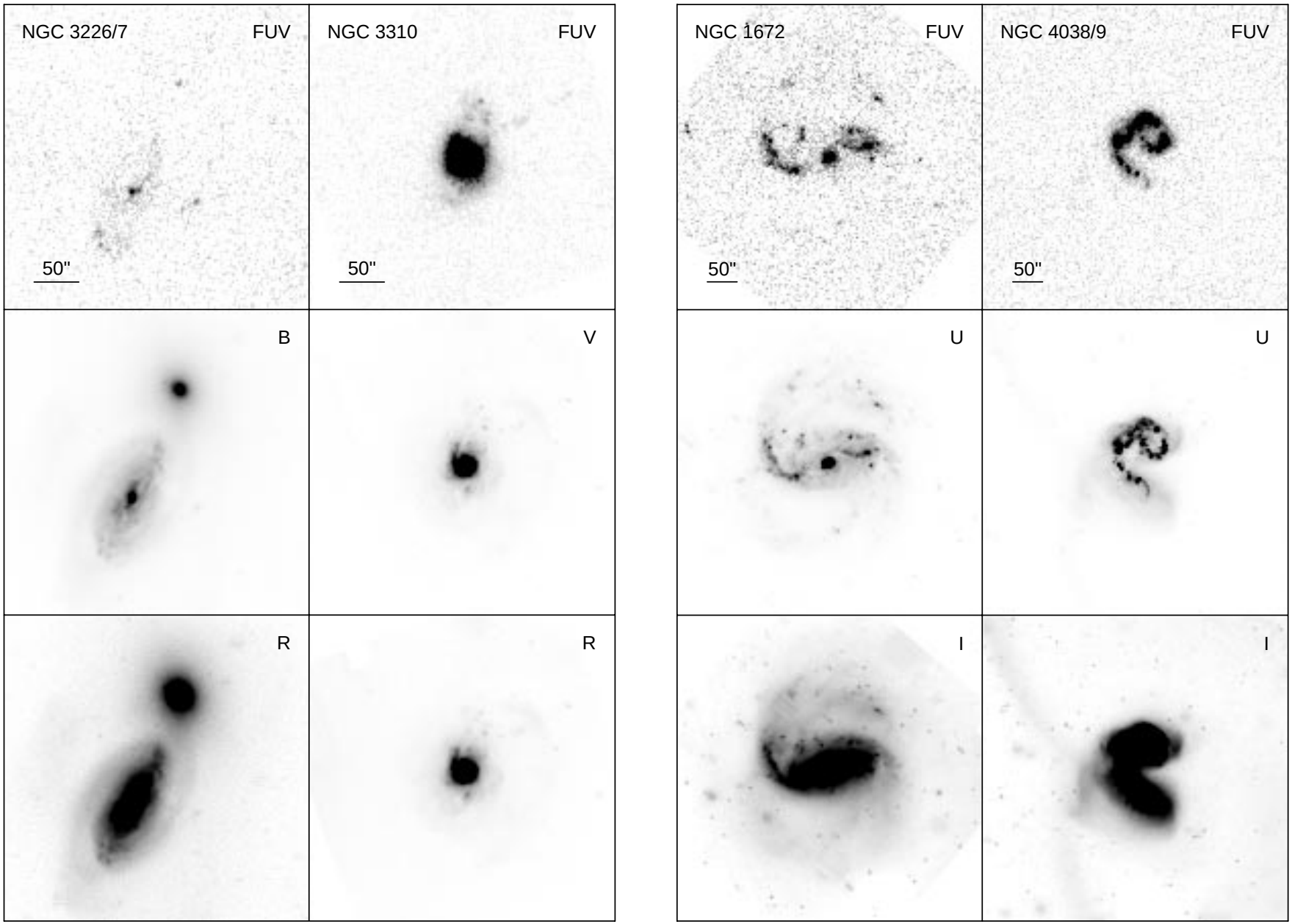

FIG. 1.—*Continued*

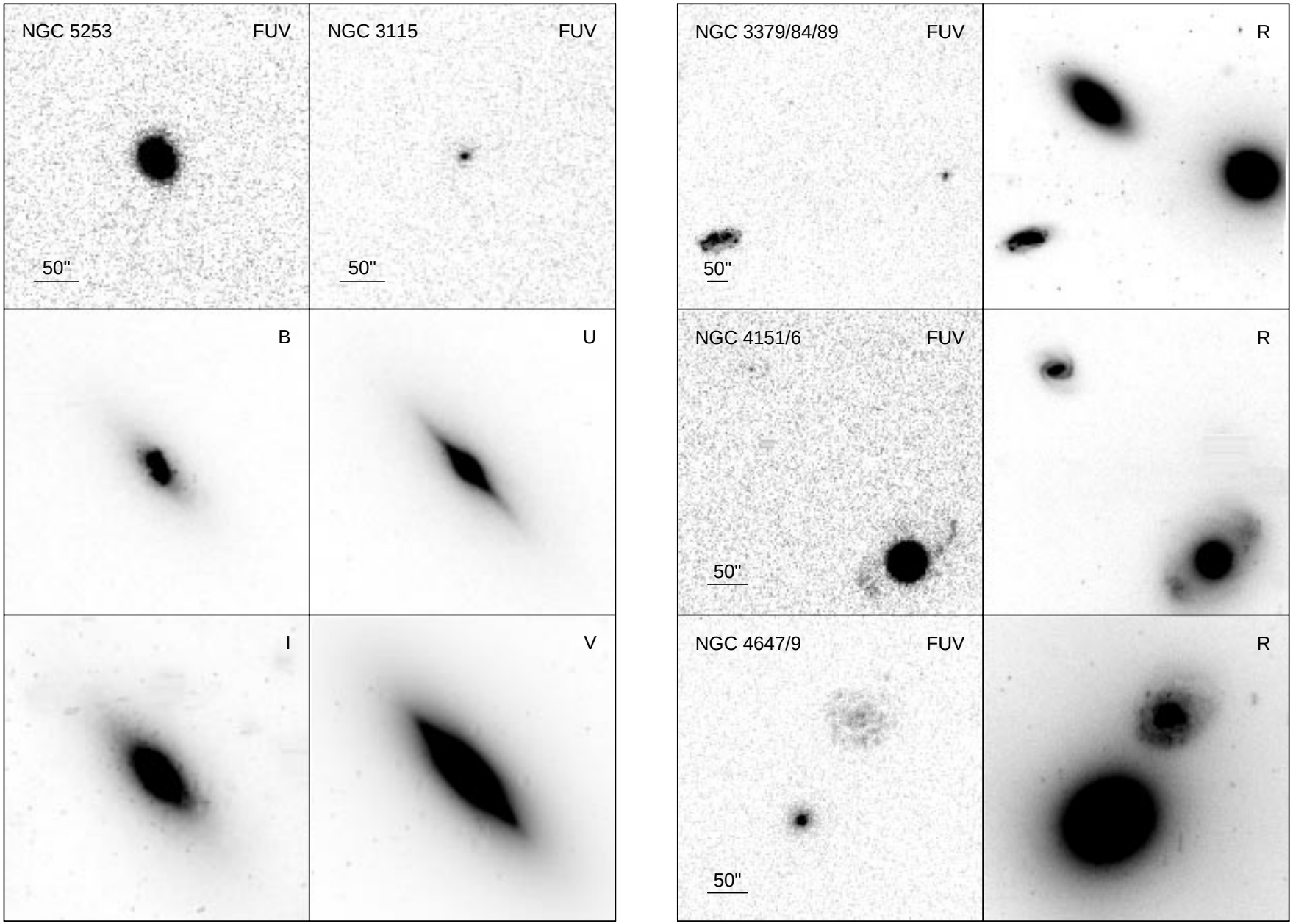

FIG. 1.—*Continued*

examining the residuals as a function of $B-V$ or $V-I$ color for those galaxies with sufficient published data over a range of colors, we found no strong evidence for color terms in the calibration. Therefore, we simply used the mean difference between the measured and published magnitudes as a calibration constant. For images in which the galaxy center was saturated, we compared the observed and published magnitudes in annuli between the smallest published aperture that enclosed all the saturated pixels and subsequent apertures. The typical scatter around this mean difference ranges from 0.02 to 0.15 mag., which is not unexpected for a mix of photometric and nonphotometric data from several different instruments. The uncertainty in optical aperture magnitudes due to sky and instrument noise is typically $\leq 3\%$. If no catalog data was available for a particular galaxy/filter, we substituted an average of the calibration constants determined in that filter for other galaxies observed during the same night. Since all but one of these cases involved calibration of R- or I-band data, airmass differences between the galaxies that were bootstrapped and those for which calibrations were determined from the literature are likely to contribute only small errors. Galaxies for which this procedure was necessary are flagged in Table 2; their calibrations are correspondingly less certain than the others. Overall, combining the noise and calibration errors, we estimate an uncertainty in the optical magnitudes of $\leq 15\%$, with the exact value for each galaxy depending on the quality of the observations and the availability of published data.

2.5. *Image Alignment and Stellar Masks*

In order to facilitate the direct comparison of galaxy morphology at UV and optical wavelengths, we transformed the coordinates of the optical data onto the system of the UIT data and smoothed all data for a particular galaxy to the same resolution. Because the FUV images contain few or no stars, the coordinates of UV-bright star-forming regions were used to determine a linear transformation (rotation, scaling, and translation) between the shortest wavelength optical image and the UIT data. After the transformation was applied to that optical image, the centroids of several bright stars were used to align additional optical data. Finally, we measured the FWHM of the PSF on each optical image and smoothed the frame to the UIT resolution of 3″. The PSF FWHM for two galaxies, M51 and NGC 925, were slightly larger than the UIT FWHM (4″ and 4″.5, respectively); in these cases the UIT images were smoothed to the optical resolution. The final images have the UIT scale of 1″.136 per pixel, implying physical scales ranging from ~ 10 to 140 pc per pixel for our sample galaxies.

Foreground stars and any remaining artifacts were masked out on the optical and FUV data before producing the images and surface brightness profiles presented in § 3. For the optical data, we identified stars on the longest wavelength image and created a mask that was used to interpolate over those pixels on all the optical images. Most of the sample galaxies lie at high Galactic latitude, so few foreground bright stars were present. However, in the case of NGC 2403, badly saturated bright stars in the R and I bands necessitated masking large areas of those images. For this galaxy, we created a separate mask for the UBV images, which did not require such extensive corrections. In a few cases it was difficult to determine whether bright spots within the galaxy were foreground stars or H II regions; here we carefully compared the optical and FUV images and masked only those spots that were not visible in the FUV. Some galaxies also required a FUV mask to interpolate over small, bright pointlike or streak artifacts (mostly due to cosmic rays) that remained after prior data processing.

3. IMAGES AND SURFACE BRIGHTNESS PROFILES

In Figure 1 we present multiwavelength images for the sample galaxies. The sky backgrounds have been removed, and foreground stars have been masked as described above. For display purposes only, image pixel values have been converted to "calibrated" flux units, such that

$$\text{mag arcsec}^{-2} = 26 - 2.5\log_{10}(\text{pixel value}) . \quad (2)$$

The images for a given galaxy are displayed using the same range of calibrated brightness for each filter, so that pixels with the same brightness (flux per Å) have a constant gray level on each image. This mode of presentation shows the relative limiting surface brightnesses of the data at different wavelengths. To conserve space, we do not show every optical image, since those from adjacent optical filters often look nearly identical. It is quite difficult to show structure simultaneously in the bright centers of galaxies and in faint outlying features, so we present additional images of some galaxies with different scales or normalizations in Figures 2 and 3. The four FUV-bright galaxies shown in Figure 2 are displayed with a much larger scale to show the central regions. In Figure 3, we show several galaxies with red FUV–optical colors, mainly early-type galaxies or those with a prominent optical bulge. Here we show the optical images with a much larger stretch than the FUV data, so that the central structure of the optical image can be compared to the FUV. We also plan to make our images available to the community in digital form via the NASA/IPAC Extragalactic Database (NED); they can then be renormalized as appropriate for any application.

We extract surface brightness profiles for each galaxy by azimuthally averaging around concentric ellipses. The ellipse center, ellipticity, and position angle (P.A.) for each galaxy were determined by running an ellipse-fitting package in VISTA (based on the method of Kent 1983) on the longest available wavelength image, usually R or I. The centroid was determined in a small box around the visual center of the galaxy, taking care to use an image in which the center was not saturated. The ellipticity and P.A. are determined from the outer ellipses, where their values were typically stable over a large range in radii. These ellipse parameters were used to obtain surface brightness profiles at all wavelengths, in order to avoid problems in determining centroids and fitting ellipses on the often asymmetric and irregular FUV images. For one galaxy, NGC 3115, we were unable to align the optical and FUV images due to a lack of bright features or foreground stars in the FUV. We determined a separate FUV ellipticity and P.A. for this galaxy using the ellipse-fitting routine. The ellipticity and P.A. for each galaxy, which are given in Table 1, are quite similar to the RC3 (de Vaucouleurs et al. 1991) values ($\Delta\epsilon \sim 0.05$ and $\Delta\text{P.A.} \leq 15°$). The surface brightness profiles derived for each sample galaxy are shown in Figure 4, with data from the various filters denoted by different symbols. Images in which the galaxy center was saturated are identifiable by their flat profiles in the central regions; this is the

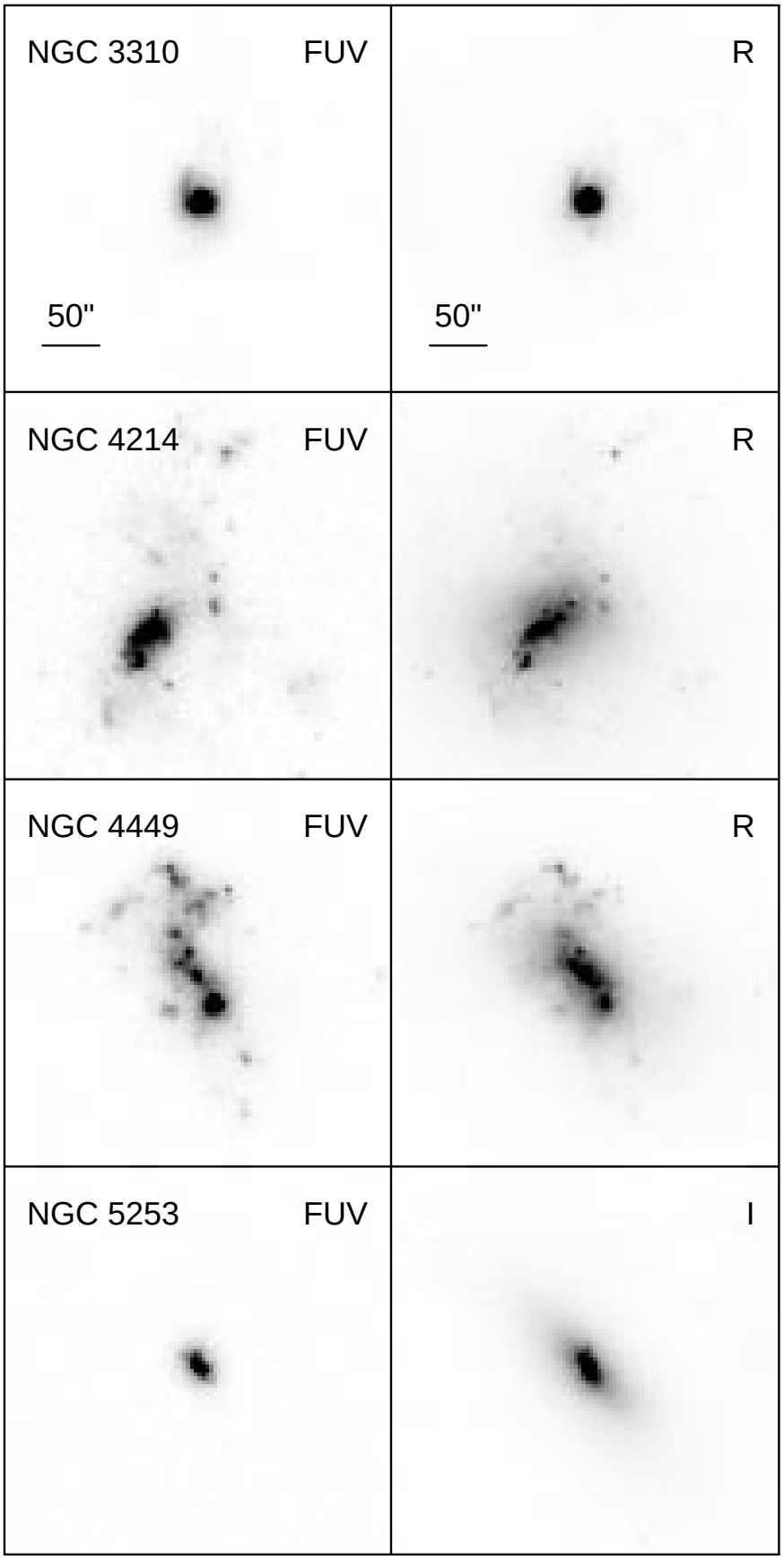

FIG. 2.—FUV and optical images of FUV-bright galaxies rescaled to show bright central regions. As in Fig. 1, pixels of the same brightness have constant gray level on all images of a galaxy.

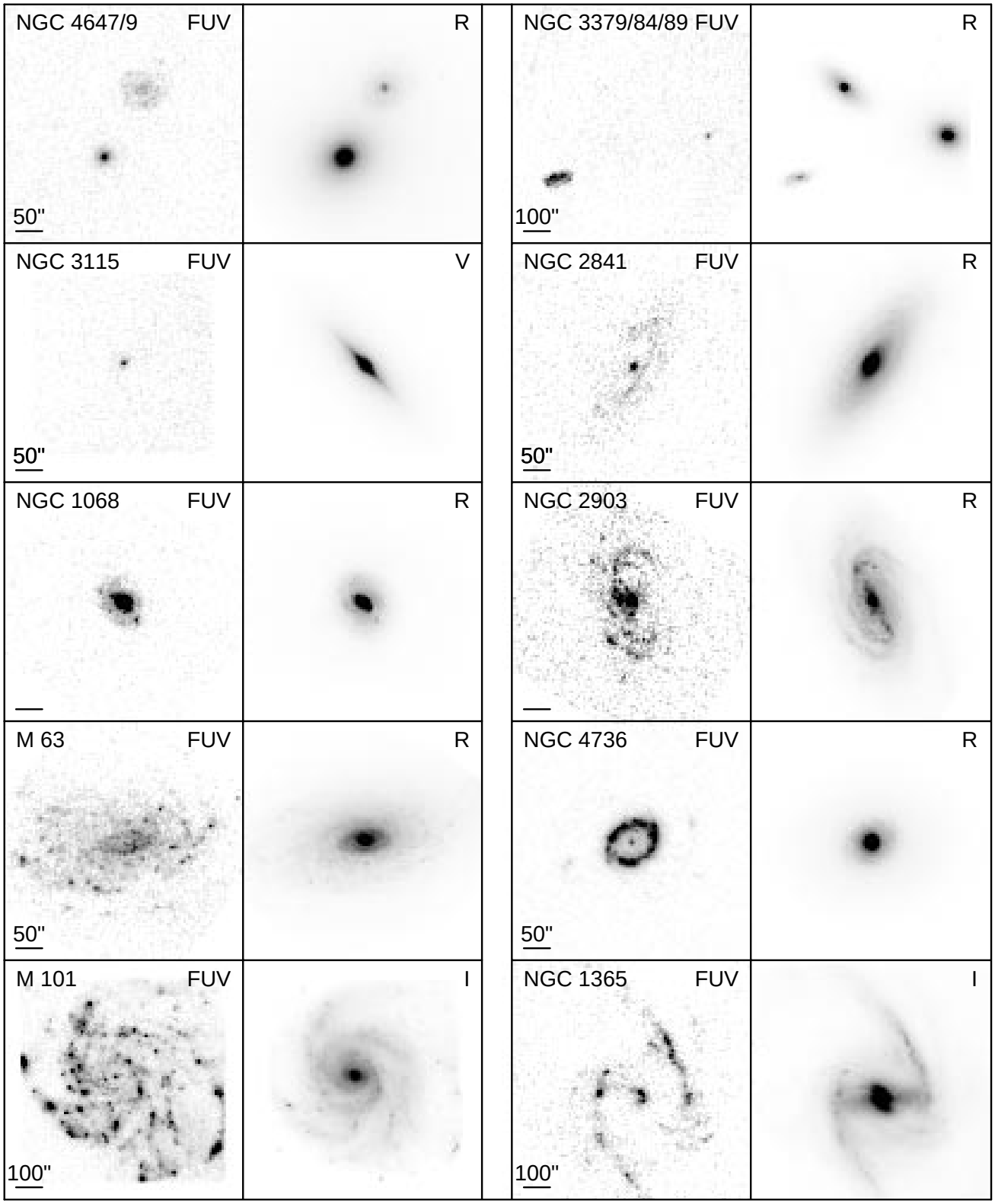

FIG. 3.—FUV and optical images of galaxies with red FUV–V colors, renormalized so that optical data are not badly saturated in the display. Here, the optical data are displayed with a larger stretch than the FUV images in order to compare the central structure in both images.

case for several optical images and the inner $\sim 10''$ of the FUV data for NGC 4151. Profiles for a subset of our sample were compared to those extracted by Fanelli et al. (1997b) from the same data; no significant differences are noted. The profiles have not been corrected for foreground Galactic extinction. However, the foreground A_B values (given in Table 1) are generally small, so even FUV extinctions of $\sim 2A_B$ amount to ≤ 0.5 mag and would have little effect on the plots of Figure 4.

Three systems in our sample are interacting pairs for which it is difficult to separate the light profiles of the two galaxies: NGC 4038/4039, NGC 3226/3227, and NGC

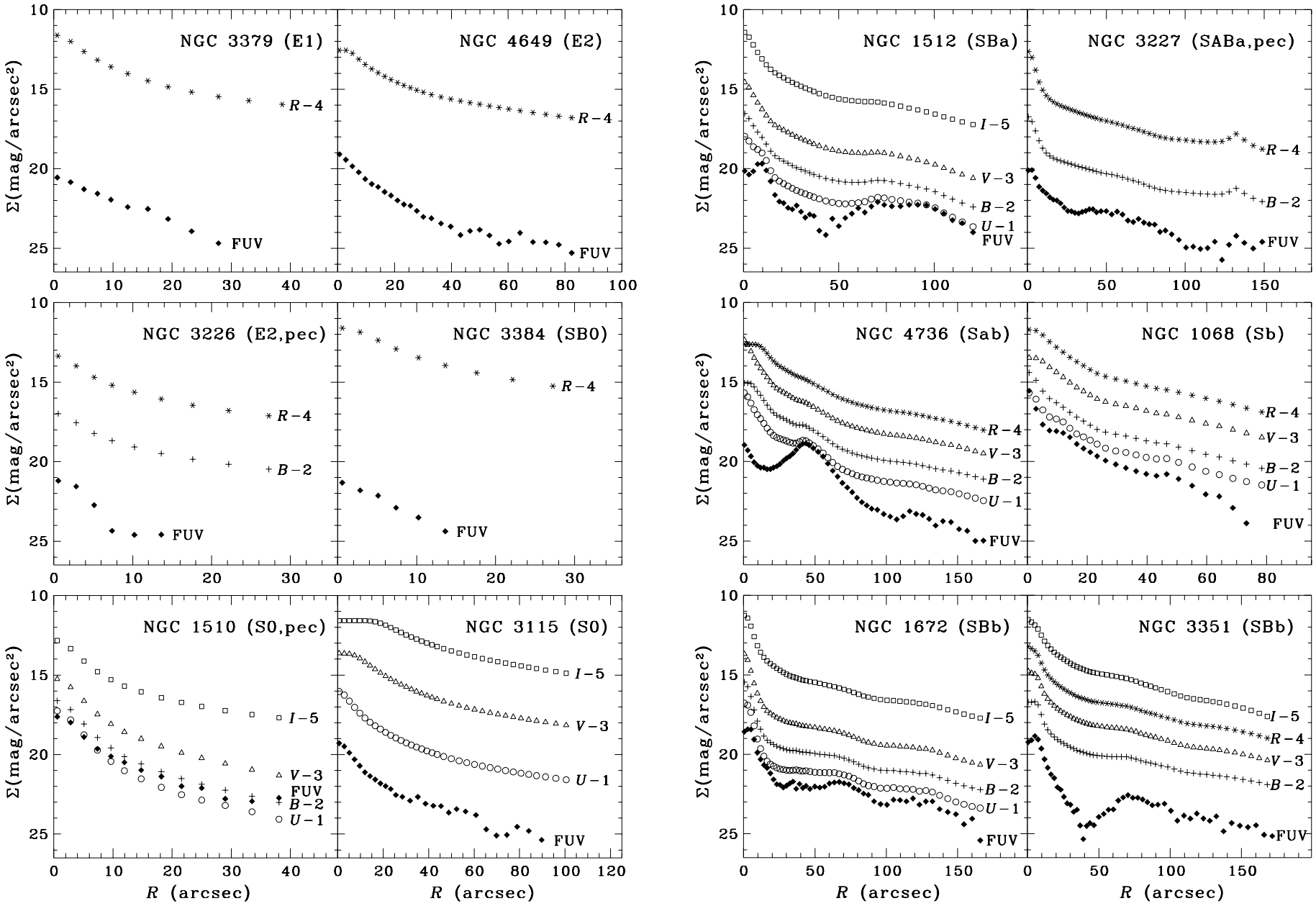

FIG. 4.—FUV and optical surface brightness profiles of sample galaxies. The surface brightnesses are calibrated as described in the text, then offset by a constant to better show the relative shapes. Data from the optical filters are offset for ease of viewing; offsets are noted on each panel. Symbols for the different filters are as follows: *filled diamonds*: FUV; *open circles*: U; *plus signs*: B; *open triangles*: V; *asterisks*: R; *open squares*: I.

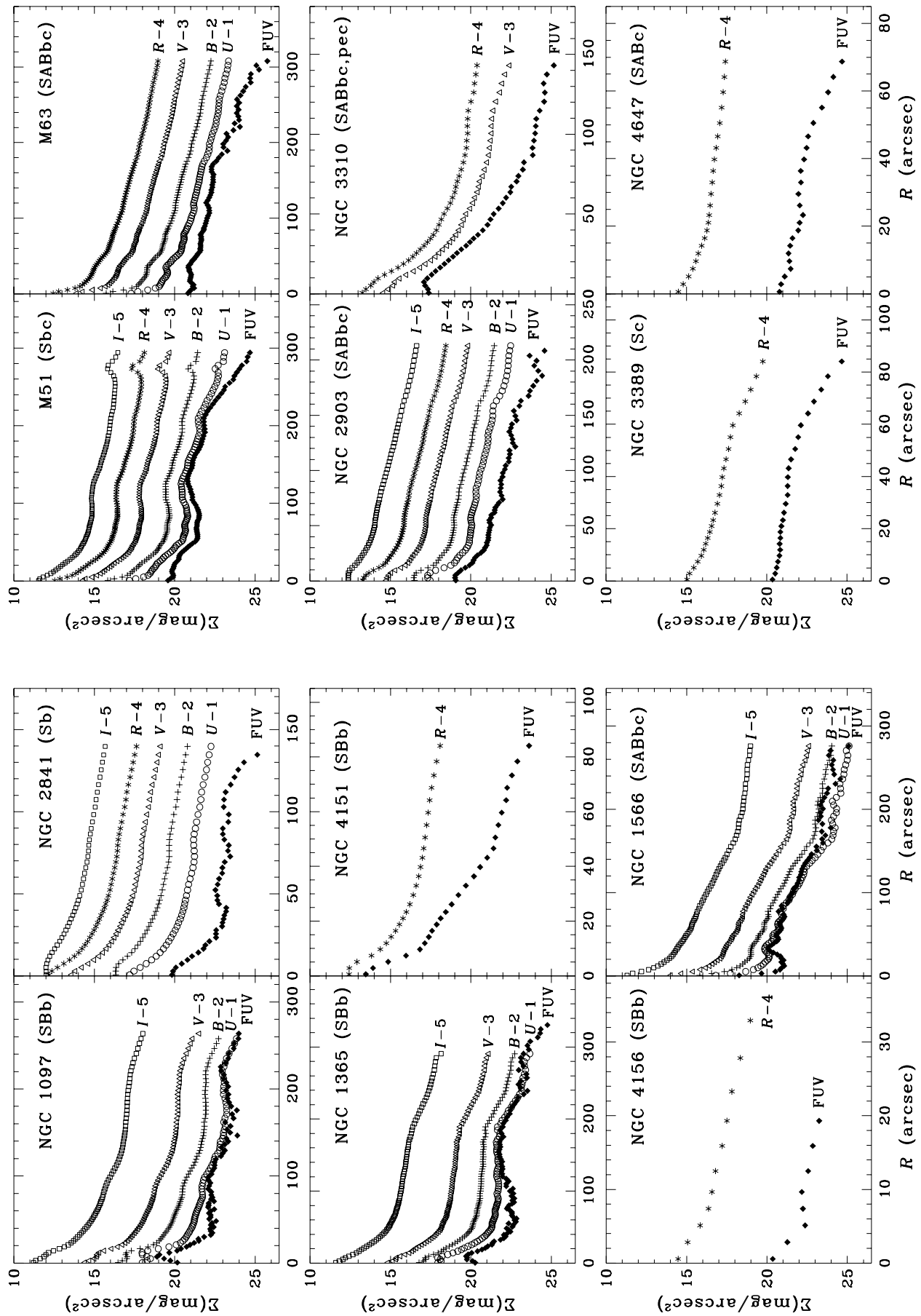

FIG. 4.—*Continued*

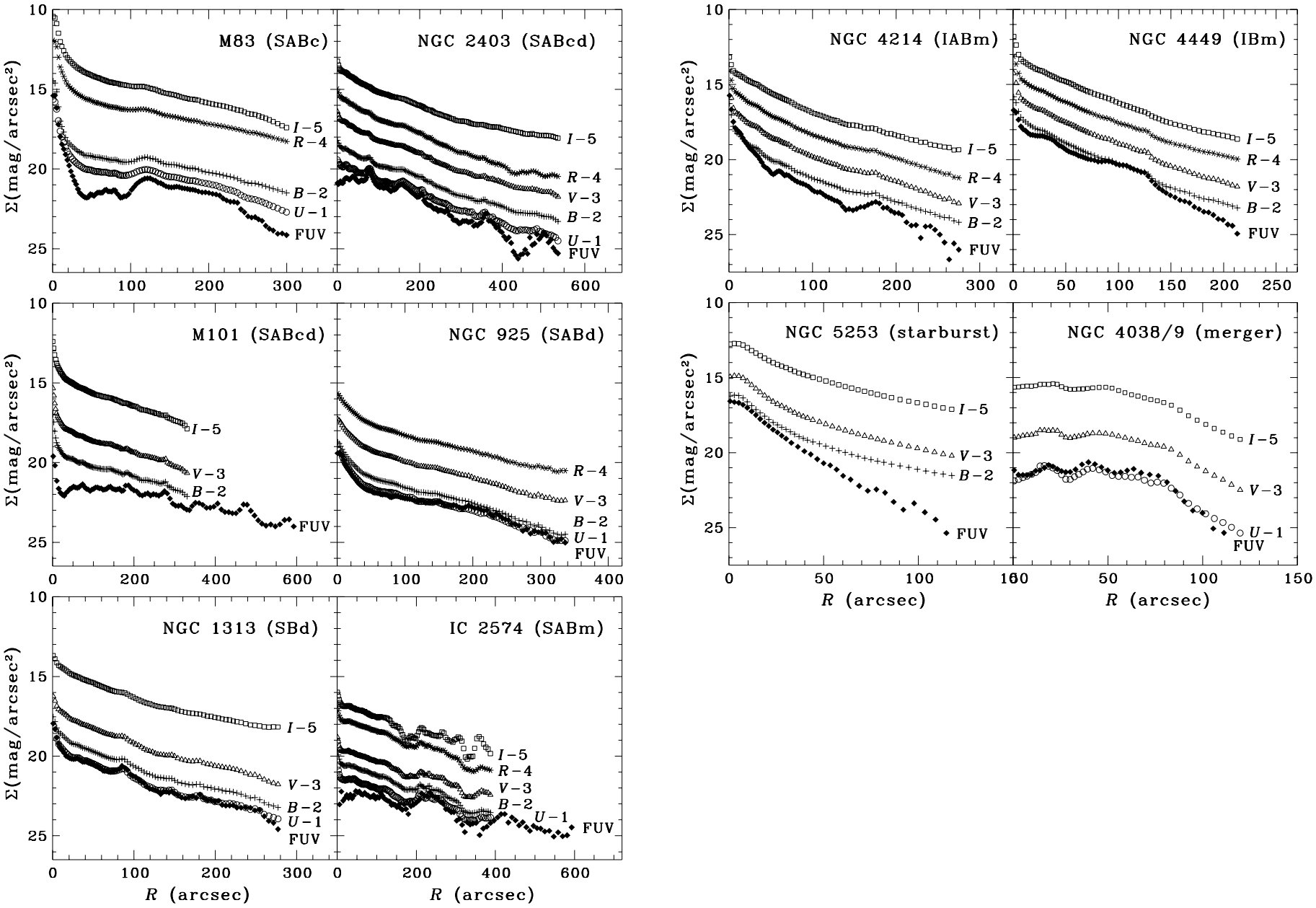

FIG. 4.—*Continued*

TABLE 1

BASIC DATA FOR UIT SAMPLE GALAXIES

Name	α (2000)[a]	δ (2000)[a]	Type[b]	Activity[b]	D[c]	A_B[d]	ϵ[e]	P.A.[f]
NGC 925	02 27 16.8	+33 34 41	SAB(s)d	...	9.4	0.25	0.40	115
NGC 1068 (M 77)	02 42 40.2	−00 00 48	RSA(rs)b	Sy 2	14.4	0.05	0.20	84
NGC 1097	02 46 18.9	−30 16 21	SB(s)b	Sy 1	14.5	0.07	0.32	140
NGC 1313	03 18 15.5	−66 29 51	SB(s)d	...	3.7	0.03	0.20	40
NGC 1365	03 33 36.6	−36 08 17	SB(s)b	Sy 1.8	16.9	0.00	0.45	32
NGC 1510	04 03 32.6	−43 24 01	S0, pec	H II	10.3	0.00	0.12	115
NGC 1512	04 03 54.6	−43 21 03	SB(r)a	...	9.5	0.00	0.36	56
NGC 1566	04 20 00.4	−54 56 18	SAB(s)bc	Sy 1	13.4	0.00	0.21	40
NGC 1672	04 45 42.2	−59 14 57	SB(s)b	Sy 2	14.5	0.00	0.13	161
NGC 2403	07 36 54.5	+65 35 58	SAB(s)cd	...	4.2	0.16	0.44	115
NGC 2841	09 22 01.8	+50 58 31	SA(r)b	LINER, Sy 1	12.0	0.00	0.56	147
NGC 2903	09 32 09.7	+21 30 02	SAB(rs)bc	H II	6.3	0.07	0.53	24
NGC 3115	10 05 14.1	−07 43 07	S0	...	6.7	0.10	0.66[g]	43[f]
NGC 3226	10 23 27.4	+19 53 55	E2*, pec	LINER	23.4	0.02	0.20	10
NGC 3227	10 23 31.5	+19 51 48	SAB(s)a,pec	Sy 1.5	20.6	0.02	0.55	157
IC 2574	10 28 22.5	+68 24 39	SAB(s)m	...	2.7	0.06	0.59	62
NGC 3310	10 38 46.1	+53 30 08	SAB(r)bc, pec	H II	18.7	0.00	0.22	170
NGC 3351 (M 95)	10 43 58.0	+11 42 15	SB(r)b	H II	8.1	0.04	0.32	17
NGC 3379 (M 105)	10 47 49.9	+12 34 57	E1	...	8.1	0.05	0.13	65
NGC 3384	10 48 17.2	+12 37 49	SB0*	...	8.1	0.05	0.50	51
NGC 3389	10 48 27.9	+12 32 01	SA(s)c	...	22.5	0.06	0.55	108
NGC 4038	12 01 52.9	−18 51 54	SB(s)m, pec	...	25.5	0.05	0.00[h]	...
NGC 4039	12 01 53.9	−18 53 06	SA(s)m, pec	...	25.3	0.05	0.00[h]	...
NGC 4151	12 10 33.0	+39 24 28	SAB(rs)ab*, pec	Sy 1.5	20.3	0.00	0.36	145
NGC 4156	12 10 49.7	+39 28 24	SB(rs)b	LINER	90.4[i]	0.00	0.20	45
NGC 4214	12 15 39.5	+36 19 39	IAB(s)m	H II	3.5	0.00	0.18	132
NGC 4449	12 28 11.4	+44 05 40	IBm	...	3.0	0.00	0.46	60
NGC 4647	12 43 32.4	+11 34 56	SAB(rs)c	...	16.8	0.04	0.20	135
NGC 4649 (M 60)	12 43 40.3	+11 32 58	E2	...	16.8	0.04	0.17	130
NGC 4736 (M 94)	12 50 53.6	+41 07 10	(R)SA(r)ab	LINER	4.3	0.00	0.22	95
NGC 5055 (M 63)	13 15 49.3	+42 02 06	SA(rs)bc	H II, LINER	7.2	0.00	0.47	102
NGC 5194 (M 51)	13 29 53.3	+47 11 48	SA(s)bc, pec	Sy 2.5	7.7	0.00	0.30	30
NGC 5236 (M 83)	13 37 00.3	−29 52 04	SAB(s)c	H II	4.7	0.14	0.10	80
NGC 5253	13 39 55.9	−31 38 41	Pec	H II	3.2	0.19	0.57	43
NGC 5457 (M 101)	14 03 12.5	+54 20 55	SAB(rs)cd	...	5.4	0.00	0.00	...

[a] Data from the RC3.
[b] Nuclear activity classification, from the NASA Extragalactic Database (NED).
[c] Distances in Mpc from Tully 1988 ($H_0 = 75$ km s^{-1} Mpc^{-1}), except as noted.
[d] Foreground Galactic extinction values from Burstein & Heiles 1984.
[e] Adopted ellipticity for azimuthal averaging in surface brightness profile calculations, defined as $\epsilon = 1 - (b/a)$.
[f] Adopted major-axis position angle for azimuthal averaging in surface brightness profile calculations.
[g] An ellipticity of 0.29 and a P.A. of 118 were used for the FUV image of NGC 3115, which was never registered to the optical data (see § 3).
[h] NGC 4038/4039 is treated as one galaxy for profile calculation; see § 3.
[i] Distance from V_{GSR}, $H_0 = 75$ km s^{-1} Mpc^{-1}.

5194/5195 (M51a, b). (NGC 4647 and NGC 4649 are a close pair that may be undergoing a mild interaction, but their FUV isophotes do not overlap in our images.) For NGC 5194/5195, the companion galaxy NGC 5195 is undetected in the FUV image and thus is not analyzed separately. The ellipse parameters for NGC 5194 are determined from a region unaffected by the companion on the optical images. Many of the outer ellipses cut through the companion, creating a slight "bump" in the outer part of the optical surface brightness profiles. The outer ellipses for NGC 3227 encompass all the FUV light and a significant fraction of the optical light of its companion, NGC 3226. Within the available software packages, it is impossible to avoid this situation without either severely truncating the NGC 3227 profile or changing the ellipticity so much that it no longer accurately reflects the shape of NGC 3227. However, the NGC 3226 profile of the region with detectable FUV emission is relatively unaffected. The merger system NGC 4038/4039 is treated as one galaxy, since the FUV image does not suggest a simple division into two separate disks. We created an image of this system consisting of only pixels with flux greater than $1.5\sigma_{sky}$ above the background that also have at least four adjacent pixels above the threshold. ("Adjacent" pixels are defined as those that share either an edge or a corner with the pixel in question; thus, each pixel has eight adjacent neighbors.) This image is approximately circular, so we defined an aperture center at the geometric center of the FUV image and used circular annuli to measure the light profiles.

Color profiles are produced by subtracting the surface brightness profiles (in mag arcsec^{-2}) of different filters. The use of a single set of ellipse parameters for all images of a particular galaxy ensures that the light profiles at each wavelength sample the same physical region and thus can

TABLE 2

OBSERVATIONS OF SAMPLE GALAXIES

Name	UV Date	UV (Filter)[a]	Optical Date	Telescope[b]	U[a]	B[a]	V[a]	R[a]	I[a]
NGC 925	950314	1591 (B5)	990207	Pal 1.5	...	...	...	300[c]	...
			990213	Pal 1.5	3600[c]	600	600	...	...
NGC 1068	950307	753 (B5)	990214	Pal 1.5	3600	300	300	200	...
NGC 1097[d]	950312	1121 (B5)	951221	LCO 2.5	3 × 400	3 × 200	3 × 200	...	3 × 200
NGC 1313[d]	950312	1071 (B5)	951224	LCO 2.5	2 × 400	2 × 200	2 × 200	...	2 × 200
NGC 1365[d]	950315	974 (B5)	951223	LCO 2.5	2 × 400	2 × 200	2 × 200	...	2 × 200
NGC 1512[d]/1510[e]	950315	949 (B5)	951220	LCO 2.5	3 × 400	3 × 200	3 × 200	...	3 × 200
NGC 1566	950316	1391 (B5)	951222	LCO 2.5	2 × 400	2 × 200	2 × 200	...	2 × 200
NGC 1672	950307	927 (B5)	951219	LCO 2.5	4 × 400	3 × 200	3 × 200	...	3 × 200
NGC 2403[d]	950308	772 (B1)	971031	Pal 1.5	1600	600	300	...	300
			990208	Pal 1.5	...	...	...	60	...
NGC 2841	950308	1021 (B1)	940214	Pal 5.0	...	300	...	...	120, 2 × 60
			990213	Pal 1.5	3600	...	300	200	...
NGC 2903	950307	549 (B1)	951123	Pal 1.5	...	900	600	...	600
			990208	Pal 1.5	...	...	...	300	...
			990214	Pal 1.5	3600	...	...	...	...
NGC 3115	950307	1081 (B1)	951226	LCO 2.5	300	...	300	...	300
NGC 3226/3227[e]	950316	1271 (B1)	960218	Pal 1.5	...	450	...	...	...
			990207	Pal 1.5	...	...	...	300	...
IC 2574[d]	950316	624 (B1)	960414	Pal 5.0	...	...	3 × 600	...	5 × 400[c]
			990208	Pal 1.5	...	...	...	300[c]	...
			990214	Pal 1.5	3600	600	...	...	...
NGC 3310	950311	1131 (B1)	990207	Pal 1.5	...	...	...	300[c]	...
			990214	Pal 1.5	...	...	300	...	...
NGC 3351	950306	881 (B1)	960118	Pal 1.5	...	600	300	...	2 × 600, 300
			990208	Pal 1.5	...	...	...	300[c]	...
NGC 3379/3384/3389[e]	950306	1301 (B1)	990208	Pal 1.5	...	...	...	120	...
NGC 4038/4039[d]	950307	881 (B1)	951222	LCO 2.5	1200	...	600	...	600
NGC 4151/4156 [e]	950313	833 (B1)	990207	Pal 1.5	...	...	...	300	...
NGC 4214	950313	1061 (B1)	960514	Pal 1.5	...	600	2 × 300	...	300[c]
			990208	Pal 1.5	...	...	...	300[c]	...
NGC 4449	950307	987 (B1)	960515	Pal 1.5	...	600	300	...	300
			990207	Pal 1.5	...	...	...	300	...
NGC 4647/4649[e]	950311	1301 (B1)	990207	Pal 1.5	...	...	...	300	...
NGC 4736	950312	1041 (B1)	990208	Pal 1.5	...	2 × 600	...	300[c]	...
			990213	Pal 1.5	3600	...	...	...	...
			990320	Pal 1.5	...	...	300	...	...
NGC 5055[d]	950315	1141 (B1)	990213	Pal 1.5	3600	600	300	200	...
NGC 5194[d]	950312	1101 (B1)	980423	Pal 1.5	6 × 1800	...	...	...	...
			990207	Pal 1.5	...	900	600	300	300
NGC 5236[d]	950306	819 (B1)	960623	CTIO 1.5	4 × 300	4 × 300	...	4 × 300	4 × 60
NGC 5253	950307	727 (B5)	951222	LCO 2.5	...	300	...	...	...
			951223	LCO 2.5	...	...	3 × 600	...	2 × 600
NGC 5457[d]	950311	1311 (B1)	960515	Pal 1.5	...	600	300	...	300

[a] Exposure time in seconds (UV filter in parentheses).
[b] LCO 2.5: Las Campanas 2.5 m; CTIO 1.5: Cerro Tololo 1.5 m, Pal 5.0: Palomar 5 m; Pal 1.5: Palomar 1.5 m.
[c] Calibration estimated from other galaxies observed on the same night (see § 2.4).
[d] Optical sky background uncertain because galaxy fills the frame.
[e] Galaxies imaged on same frame.

be compared in this simple manner. Color profiles for many of the sample galaxies will be presented and discussed in the next section.

4. OPTICAL AND FUV MORPHOLOGY

In this section we present a qualitative discussion of the differences in apparent morphology between FUV and optical images. The morphological types included in each subsection below are approximate, stemming in part from the fact that several galaxies have characteristics associated with more than one "type". Rather than discussing each galaxy individually (as is done in Marcum et al. 2000), we summarize the changes in apparent morphology with wavelength for various Hubble types. (Interested readers can see the results for each individual galaxy from the data presented in Figure 1.) Throughout this section, we also consider implications of our analysis for the study of high-redshift galaxies that are observed in their rest-frame UV. It is important to remember that this level of discussion assumes no evolution of the star-formation rate: we simply consider what galaxies *identical* to local ellipticals, spirals, and irregulars would look like at high redshift. Galaxies undergoing their initial starburst or a subsequent period of increased star formation activity due to mergers, etc. would,

of course, look different from the quiescent ellipticals and "normal" spirals in this sample and may more closely resemble star-forming irregular or peculiar systems.

4.1. *Elliptical and S0 Galaxies*

The elliptical and S0 galaxies in our sample feature smooth, compact FUV emission centered on the nuclear regions (see also the detailed analysis of UIT data for E/S0 galaxies in Ohl et al. 1998). In galaxies of this type, FUV emission is produced not by young stars but by the hot, evolved population responsible for the spectrosopic UV upturn (O'Connell 1999). The FUV light profiles of these systems (NGC 3379, NGC 3384, NGC 4649, NGC 3226, and NGC 3115) drop off much more rapidly than the optical light, and the colors throughout are quite red (FUV–$R \sim 2$–5). FUV half-light radii for these galaxies are $\sim$20%–35% of their B-band values tabulated in the RC3 (we cannot compare directly to our optical data because most of the E/SO optical images suffer saturation in the center). The only exception to this pattern is NGC 1510, the interacting companion of NGC 1512. The FUV emission in this galaxy is comparable to the optical light in both brightness and physical extent, and is likely due to tidally induced star formation rather than the evolved population. Although it is classified in the RC3 as a peculiar S0 galaxy, Sandage & Brucato (1979) classify NGC 1510 as an amorphous galaxy, and it is also noted to be a star-forming blue compact dwarf (BCD) in Kinney et al. (1993) and an H II galaxy in NED. (The other S0/amorphous galaxy in our sample, NGC 5195, is also interacting with companion galaxy NGC 5194, but is not detected in the FUV.)

It is difficult to predict the appearance of high-redshift E/S0 galaxies in their rest-frame FUV because the present-day UV emission mechanism, that of evolved stars, is likely to be weak to nonexistent at redshifts approaching $z \sim 1$ (Brown et al. 1998, 2000). Indeed, the UV upturn phenomenon is a potentially sensitive age indicator for evolved stellar populations, and thus its evolution with redshift could help identify the formation epoch of early-type galaxies (Yi et al. 1999). At high redshifts, ellipticals may be undergoing an initial starburst and/or the UV upturn population will not yet have had time to evolve. In this case, the progenitors of present-day elliptical and S0 galaxies may look like local starbursts or mergers, depending on their formation mechanism and the timing of the observations. However, if some high-redshift E/S0's were quiescent and identical to local early-type galaxies (i.e., assuming a very high formation redshift), they would still have the smooth and symmetric light distributions associated with early types. Their FUV emission would be much more compact than the optical light, which would lead to difficulties in detection and confusion in estimating their typical size.

4.2. *Early-Type Spiral Galaxies*

Galaxies of Hubble type Sa-Sbc tend to appear as later type spirals in the FUV than at optical wavelengths, primarily due to fading of the red bulge and bar in UV images. A significant fraction of the FUV light in these systems comes from star-forming regions in the spiral arms, which are visible in the images of Figure 1 and appear as "bumps" in the FUV surface brightness profiles of Figure 4 (see also Fanelli et al. 1997b). Some early-type spirals, such as M63 and NGC 1672, also appear more patchy or fragmented in the FUV because old stars in the underlying smooth disk do not produce much light at very short wavelengths. These results are in agreement with earlier work by O'Connell (1997a) and O'Connell & Marcum (1996) for smaller samples of galaxies. The dramatic fading of light in the central regions (also noted by O'Connell 1997a and Waller et al. 1997b) produces a global pattern in which the central FUV–optical colors are much redder than the outer regions, as shown in Figure 5 for M51, NGC 1566, and M63. Two notable exceptions to this pattern are NGC 4151, in which the Seyfert 1 nucleus dominates the central FUV emission and is much brighter than the weak spiral arms, and NGC 1068, in which the FUV-bright Seyfert 2 nucleus and surrounding star formation combine to produce a very blue center. The UV morphologies and luminosities of the AGN and star-forming components in these two galaxies are discussed in more detail by Fanelli et al. (1997a).

Many early-type spirals also show evidence of star-forming inner rings or circumnuclear star formation, which often dominate the FUV images and light profiles. Images of these features, which are present in NGC 1097, NGC 1512, NGC 1672, NGC 3310, NGC 3351, and NGC 4736, are shown in Figure 6, and the associated color profiles are plotted in Figure 7. The star-forming rings appear as spikes of FUV brightness or very blue color in the radial profiles of Figures 4 and 7. Inner and circumnuclear rings are thought to be orchestrated by dynamical resonances, which are often associated with central bars (e.g., Storchi-Bergmann, Wilson, & Baldwin 1996; Buta & Combes 1996). The FUV properties of some specific ringed galaxies are discussed by Waller et al. (1997c, 2000) for NGC 4736, Smith et al. (1996) for NGC 3310, and P. M. Marcum et al. (in preparation).

Galaxies classified from their optical images as early-type spirals may present a variety of different appearances when viewed at high redshift, in their rest-frame FUV. Optically barred galaxies such as NGC 1097 and NGC 1365 will appear unbarred in the ultraviolet. Isolated galaxies such as NGC 1672 that appear highly fragmented in the FUV may be mistaken for an ongoing merger. Images of distant systems may recover only the FUV-bright star-forming rings or circumnuclear star formation, yielding little evidence of the underlying regular structure seen in the

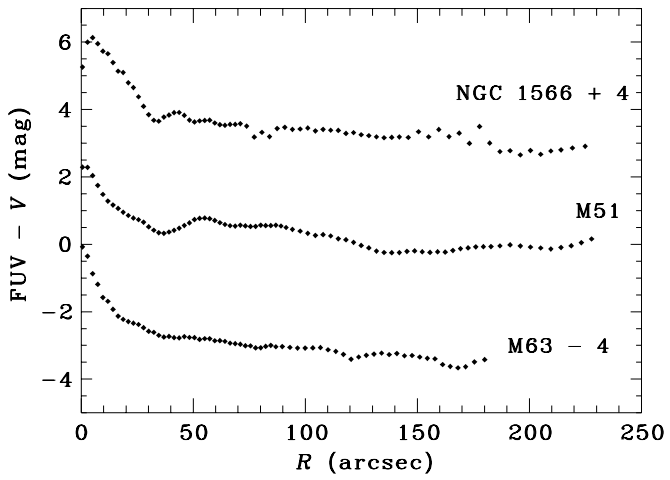

FIG. 5.—FUV–optical color profiles for early-type spiral galaxies. The galaxy name and constant offset (where applicable) are noted next to each profile.

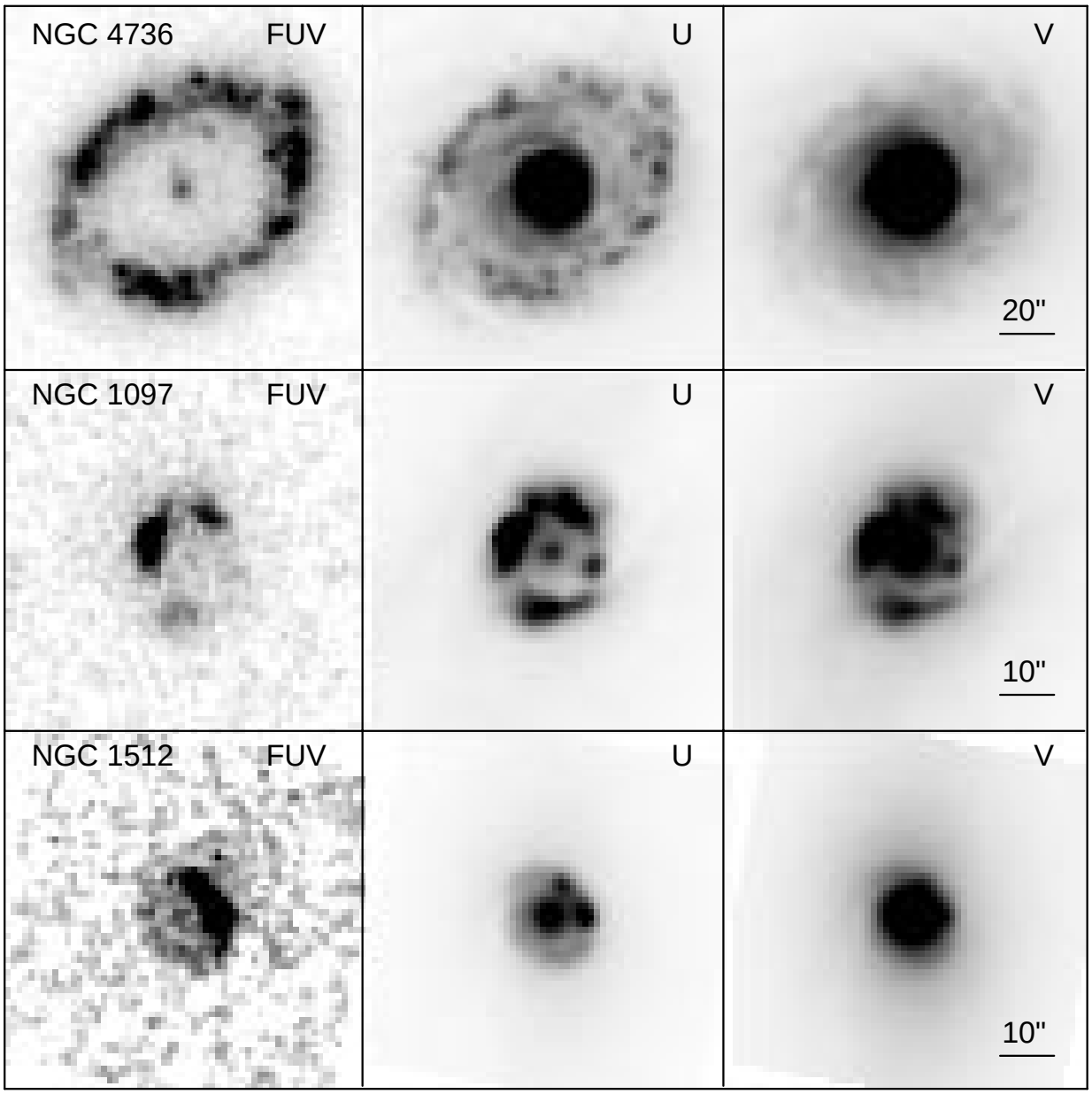

FIG. 6.—FUV and optical images of circumnuclear and inner star-forming rings in early-type spirals. The images are aligned, oriented, and scaled as described in Fig. 1.

galaxy's optical light (see also Waller et al. 1997b). On the other hand, galaxies such as NGC 4151 appear to have an earlier morphological type in the FUV due to the prominence of highly symmetric and strongly peaked emission from the active nucleus. Finally, the appearance of a galaxy undergoing a global starburst, such as NGC 3310, does not differ a great deal between the FUV and optical because the light at both wavelengths is dominated by young stars. We have found that all these effects can vary in magnitude, such that some galaxies would be assigned nearly the same Hubble type in the optical and FUV, while others would have very different classifications. Overall, most optically classified early-type spirals present the appearance of a later type in the FUV, but a small fraction may appear to have identical or earlier FUV types in the presence of starburst activity or an AGN.

4.3. *Late-Type Spirals, Irregulars, and Starbursts*

Galaxies that are optically classified as late-type spirals generally do not show as dramatic a difference between their FUV and optical morphologies as do early-type spirals. Although they often appear somewhat more patchy in the FUV, there is no prominent optical bulge whose absence at short wavelengths is noticeable. Star formation occurs over a large fraction of the galaxy, producing both FUV and optical light in the same physical regions. A number of these galaxies, including NGC 4449, NGC 925, NGC 1313, and IC 2574, show color profiles that have no definite trend with radius. These profiles, examples of which are displayed in Figure 8, are either flat or bumpy depending on the relative prominence of star-forming regions against the background disk. Figure 9 shows color profiles

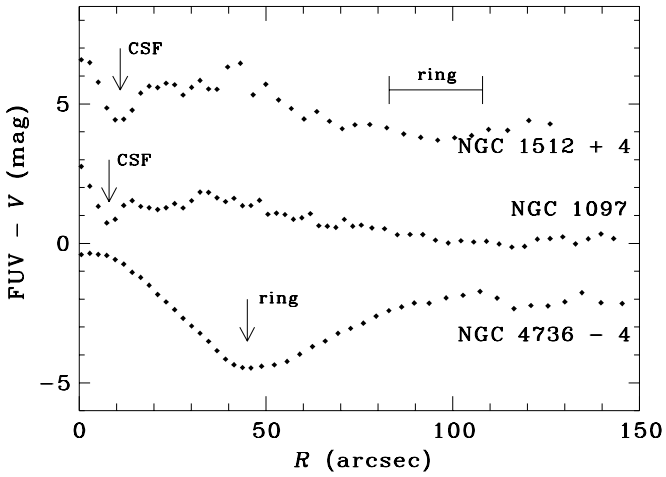

FIG. 7.—Color profiles for early-type spirals with star-forming rings or circumnuclear star formation. As in Fig. 5, the galaxy name and constant offset are noted next to each profile. Locations of the rings and circumnuclear star formation (CSF) regions are labeled for each galaxy.

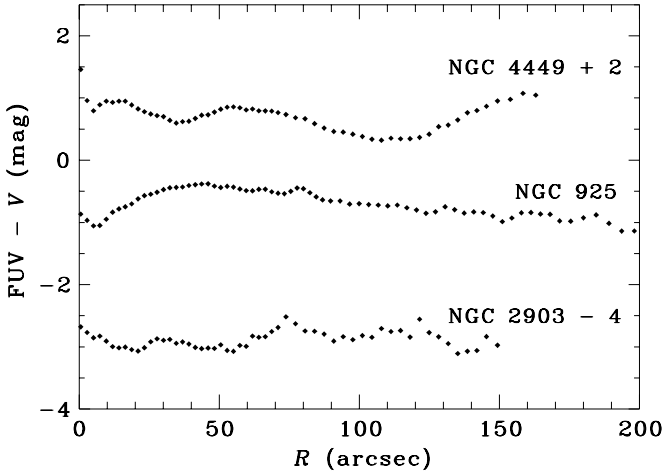

FIG. 8.—Color profiles for late-type galaxies with flat FUV–optical color gradients. As in Fig. 5, the galaxy name and constant offset are noted next to each profile.

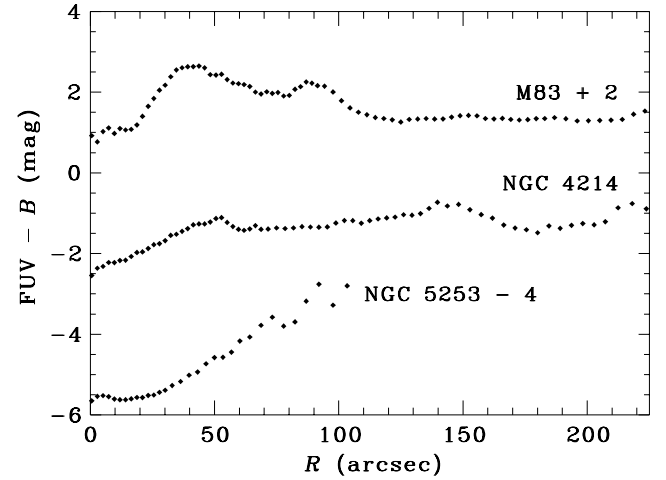

FIG. 9.—Color profiles for late-type galaxies with central starbursts. As in Fig. 5, the galaxy name and constant offset are noted next to each profile.

for the central starburst galaxies M83, NGC 4214, and NGC 5253, which are bluest in their centers. NGC 4214 and NGC 5253 have global color gradients in the opposite direction to that observed in early-type spirals, due to the presence of a blue starburst superposed on a more extended old stellar distribution. This "starburst core" morphology has been previously noted in FUV–optical image comparisons of NGC 4214 (Fanelli et al. 1997c) and NGC 5253 (Kinney et al. 1993). A central starburst combined with bright star-forming regions in the outer disk can also produce a flat color profile, which is the case for NGC 2903 (also shown in Fig. 9).

We find that the morphological *k*-correction for late-type galaxies is expected to be highly dependent on whether or not they host starburst activity. As is evident from their similar FUV and optical morphology, nonstarbursting late-type galaxies (dominated by ongoing disk star formation) viewed at high redshift would not generally appear to have a very different type from their local counterparts. Increased patchiness in the FUV (if it were still detectable at large distances) might suggest a slightly later type than the optical appearance. However, galaxies with central starbursts like those seen in NGC 4214 and NGC 5253 might present compact cores surrounded by diffuse light, similar to some objects seen on deep *HST* images (Giavalisco, Steidel, & Duccio Macchetto 1996b). The symmetric central burst in NGC 5253 might even appear to be an E or S0 galaxy in the absence of the old stars. If starburst systems are more prevalent at high redshift, their strong influence on the rest-frame UV morphology must be considered when studying the evolution of the galaxy population.

4.4. *Interacting Systems*

As might be expected, the morphological *k*-correction for interacting galaxies depends strongly on the details of the interaction itself. Three objects in our sample are currently undergoing interactions of various degrees: NGC 4038/4039 (the Antennae), NGC 3226/3227, and NGC 5194/5195 (M51). The merger of two disk galaxies in NGC 4038/4039 has produced a significant amount of massive star formation, concentrated mainly between the two disks and around the edge of the NGC 4038 disk. Thus, the FUV image shows a partial outline of the merger system, and, without the corresponding optical data, suggests the appearance of a single, drastically perturbed galaxy. However, the old populations visible in long-wavelength optical images clearly delineate the inner disks and tidal tails that identify NGC 4038/4039 as an ongoing disk-disk merger. In spite of the dramatic difference between its FUV and optical appearances, NGC 4038/4039 is clearly peculiar at both wavelengths and thus would not be misclassified as any sort of "normal" Hubble type galaxy when viewed at high redshift. Both galaxies in the NGC 3226/3227 interacting pair present FUV morphologies consistent with what would be expected from their Hubble types: the elliptical NGC 3226 appears highly concentrated and the Sa NGC 3227 shows emission from the center and a few faint disk star formation regions. In this case, the influence of the interaction in determining the FUV morphology is confined to its possible role in driving the Seyfert nucleus and circumnuclear star formation in NGC 3227 (Keel 1996; Gonzalez Delgado & Perez 1997). NGC 5195 is not detected in the FUV, likely due to obscuration by dust from a foreground spiral arm in NGC 5194 as well as possible internal

extinction (see Sandage 1961; Barth et al. 1998 also suspect that dust is responsible for their failure to detect NGC 5195 at 2200 Å). Observed at high redshift in its rest-frame UV, the M51 double-galaxy system would appear to be an isolated spiral galaxy. Although the examples discussed above demonstrate the difficulty of relating UV and optical morphology for interacting systems, interactions that are significant enough to severely distort the galaxies involved are often associated with enhanced star formation rates that may identify the system as "abnormal" in the FUV as well (Kennicutt 1998 and references therein).

4.5. *Dust and Morphology*

Throughout this section we have discussed FUV morphology mainly in terms of the current star formation, but, as suggested by the example of M51, one cannot neglect the possibility that extinction also influences the UV appearance of galaxies. It is difficult to ascertain whether the "patchiness" or fragmented appearance of many galaxies in the FUV is due to internal extinction or to the pattern of massive star formation. Two of the most highly inclined ($i \sim 65°$) galaxies in our sample, NGC 2841 and NGC 2903, have asymmetric FUV emission, with the bright side corresponding to what appears to be the unobscured side of the optical disk. On the other hand, NGC 2403 and IC 2574 also have $i \geq 60°$, but do not appear to suffer heavy extinction on one side of the disk. These results provide further confirmation of the variations in FUV brightness of edge-on galaxies noted by Smith et al. (1997, 2000) for NGC 4631 (FUV-bright) and NGC 891 (undetected). An extreme case of extinction effects was discussed above for NGC 5195 (M51b), which is completely obscured in the FUV by the foreground spiral arm of NGC 5194 (M51a). As noted in § 1, the role of dust in determining the observed FUV morphology depends strongly on the dust-star geometry of individual galaxies and is thus difficult to predict from optical images alone.

5. SUMMARY AND DISCUSSION

We have presented FUV and optical images and surface brightness profiles for 34 galaxies observed with the UIT and compared the apparent morphology at different wavelengths in the context of interpreting images of high-redshift objects. The UIT data represent the most detailed set of FUV images obtained to date for large, nearby galaxies that are well resolved. Present-day elliptical and S0 galaxies appear smooth and symmetric in FUV as well as in optical images, but they are much more compact in the FUV and may be faint and/or unresolved at high redshift unless they are actively forming stars at that particular look-back time. The majority of spiral galaxies in our sample appear to have a later Hubble type in the FUV than at optical wavelengths, due to increased patchiness in combination with the fading of light from the bulge and/or bar populations. This effect is particularly dramatic for the early-type spirals, in which bulges and often bars are prominent optical features. The optical and FUV morphologies of late-type spirals and irregular galaxies do not differ as much as the earlier types because young stars dominate the light in both spectral regimes. Some galaxies appear highly fragmented in the FUV images in spite of a regular optical morphology, making it difficult to determine from UV data alone whether they are single systems or multiple mergers. Even assuming their current rates and patterns of star formation, many spirals viewed at high redshift would be assigned later Hubble types than their local counterparts due to band-shifting effects. Bright spiral arms and central or circumnuclear starbursts and star-forming rings dominate the FUV light and FUV–optical color profiles of many galaxies. Depending on the relative geometry of dust and young stars, extinction can play a varying role (small to dominant) in determining the apparent FUV morphology. From the galaxy sample presented here, it is apparent that understanding the correlation between FUV and optical morphology depends on one's knowledge not only of the global optical Hubble type but also of smaller scale features, mostly those due to recent star formation patterns.

The fragmented appearance of many of the FUV images and the prominence of young stars in structures such as rings or fragments of spiral arms produces FUV morphologies that do not readily fit into the traditional bins of the Hubble sequence. In order to characterize rest-frame UV galaxy populations at both low and high redshift, it will be necessary to find new ways of describing the morphology that do not by default cause the majority of galaxies to fall into the "peculiar" or other catchall bins. It would also be desirable to have an objective classification scheme to express the similarities or differences between local and distant galaxies in quantitative terms. However, UV data pose problems for many automated classification schemes because galaxy centers are often ill-defined, and the patchy nature complicates the selection of an aperture that encloses a single system. Future work in this area will use UIT data to identify new features or indices that better describe the UV morphology of galaxies.

The data set presented in this paper will be valuable for studying the morphological k-correction that must be taken into account when interpreting deep optical images such as the Hubble Deep Field (HDF; Williams et al. 1996). The dependence of FUV morphology on features that are considered minor or secondary details in the optical highlights the difficulty of studying evolution in the galaxy population by comparing rest-frame UV observations of high-redshift galaxies to the optical properties of local samples. The comparison between local and distant UV galaxy images is much more direct than relying on estimates of the UV morphology extrapolated from optical light and colors (e.g., Abraham et al. 1997). Indeed, a small sample of UIT galaxy images from the Astro-1 mission has been used to simulate the appearance of high-redshift counterparts of nearby bright galaxies (Giavalisco et al. 1996a). In a subsequent paper (L. E. Kuchinski et al., in preparation), we simulate the cosmological distance effects of surface brightness dimming and loss of spatial resolution on the FUV images of our larger Astro-2 galaxy sample. These simulations provide examples of how local galaxies would appear in the HDF at redshifts of $\sim$1–4. In that paper, we also attempt to quantify the effects of band shifting and distance on morphology using simple parameters such as the central concentration and asymmetry of galaxies.

One of the primary goals of studying morphology is to infer the past or ongoing physical processes that have shaped galaxies. In combination with current knowledge about the dynamical states of nearby galaxies, our multi-wavelength data set and future UV imaging data from the GALEX sky survey (Martin et al. 1997) could be used to relate UV morphology to physical structures or properties. For example, Waller et al. (1997b, 2000) find that UV-bright

starburst rings likely result from dynamical resonances with a bar component. Thus, ring features may predict the presence of an underlying disk and bar system even in UV images that appear to be fragmented or otherwise dynamically disorganized. It would also be of interest to further investigate the suggestion of Waller et al. (1997b) that optical Hubble type may be correlated with FUV–V color (although rest-frame V-band data will not necessarily be available for high-redshift galaxies). If relations between UV morphology and physical properties can be found in local galaxies *and* be shown to extend to large look-back times, they could provide a valuable tool for studying the distant universe through rest-frame UV imaging.

The authors gratefully acknowledge the help of R. Bernstein, J. Parker, R. Phelps, and N. Silbermann for obtaining some of the optical imaging data presented here. We thank O. Pevunova for assistance with preliminary data reduction. We are also grateful to the anonymous referee for many constructive suggestions. Funding for the UIT project was provided through the *Spacelab* office at NASA Headquarters under project 440-51. W. L. F. and B. F. M. acknowledge support from the Astro-2 Guest Investigator Program through grant NAG8-1051. Some of the data presented here were obtained at CTIO, which is operated by AURA as part of NOAO under a cooperative agreement with the National Science Foundation. This research has made use of the NASA/IPAC Extragalactic Database (NED), which is operated by the Jet Propulsion Laboratory, California Institute of Technology, under contract with NASA.

REFERENCES

Abraham, R. 1998, in The Ultraviolet Universe at Low and High Redshift, ed. W. H. Waller et al. (Woodbury: AIP), 195
Abraham, R. G., Freedman, W. L., & Madore, B. F. 1997, in *HST* and the High Redshift Universe, ed. N. R. Tanvir, A. Aragon-Salamanca, & J. V. Wall (Singapore: World Scientific), 57
Abraham, R. G., Tanvir, N. R., Santiago, B. X., Ellis, R. S., Glazebrook, K. G., & van den Bergh, S. 1996, MNRAS, 279, L47
Barth, A. J., Ho, L. C., Filippenko, A. V., & Sargent, W. L. W. 1998, ApJ, 496, 133
Blecha, A., Golay, M., Huguenin, D., Reichen, D., & Bersier, D. 1990, A&A, 233, L9
Bohlin, R. C., et al. 1991, ApJ, 368, 12
Brinchmann, J., et al. 1998, ApJ, 499, 112
Brosch, N. 1999, Exp. Astron., 9, 119
Brown, T. M., Bowers, C. W., Kimble, R. A., & Ferguson, H. C. 2000, ApJ, 529, L89
Brown, T. M., Ferguson, H. C., Deharveng, J.-M., & Jedrzejewski, R. I. 1998, ApJ, 508, L139
Bunker, A. J. 1999, in The OCIW Workshop on Photometric Redshifts, ed. R. Weymann et al., in press (preprint astro-ph 9907196)
Burstein, D., & Heiles, C. 1984, ApJS, 54, 33
Buta, R., & Combes, F. 1996, Fundam. Cosmic Phys., 17, 95
Cardelli, J. A., Clayton, G. C., & Mathis, J. S. 1989, ApJ, 345, 245
Cornett, R. H., et al. 1994, ApJ, 426, 553
de Vaucouleurs, G., de Vaucouleurs, A., Corwin, H. G., Buta, R. J., Paturel, G., & Fouque, P. 1991, Third Reference Catalogue of Bright Galaxies (New York: Springer) (RC3)
Donas, J., Milliard, B., & Laget, M. 1995, A&A, 303, 661
Fanelli, M. N., Collins, N., Bohlin, R. C., Neff, S. G., O'Connell, R. W., Roberts, M. S., Smith, A. M., & Stecher, T. P. 1997a, AJ, 114, 575
Fanelli, M. N., et al. 1997b, in The Ultraviolet Universe at Low and High Redshift, ed. W. H. Waller et al. (Woodbury: AIP), 83
———. 1997c, ApJ, 481, 735
Gardner, J. P., Heap, S. R., Malumuth, E. M., Hill, R. S., & Smith, E. P. 1997, in The Ultraviolet Universe at Low and High Redshift, ed. W. H. Waller et al. (Woodbury: AIP), 429
Giavalisco, M., Livio, M., Bohlin, R. C., Duccio Macchetto, F., & Stecher, T. P. 1996a, AJ, 112, 369
Giavalisco, M., Steidel, C. C., & Duccio Macchetto, F. 1996b, ApJ, 470, 189
Gonzalez Delgado, R. M., & Perez, E. 1997, MNRAS, 284, 931
Gordon, K. D., Calzetti, D., & Witt, A. N. 1997, ApJ, 487, 625
Greason, M. R., Offenberg, J. D., Cornett, R. H., Hill, R. S., & Stecher, T. P. 1994, PASP, 106, 1151
Hill, J. K., Bohlin, R. C., & Stecher, T. P. 1984, ApJ, 277, 542
Hill, J. K., et al. 1997, ApJ, 477, 673
Hill, R. S., et al. 1998, ApJ, 507, 179
Huizinga, J. E. 1994, Ph.D. thesis, Univ. Groningen
Keel, W. C. 1996, AJ, 111, 696
Kennicutt, R. C. 1998, ARA&A, 36, 189
Kent, S. M. 1983, ApJ, 266, 562
Kinney, A. L., Bohlin, R. C., Calzetti, D., Panagia, N., & Wyse, R. F. G. 1993, ApJS, 86, 5
Kuchinski, L. E., Madore, B. F., Freedman, W. L., & Trewhella, M. 2000, AJ, in press
Kuchinski, L. E., Terndrup, D. M., Gordon, K. D., & Witt, A. N. 1998, AJ, 115, 1438
Maoz, D., Filippenko, A. V., Ho, L. C., Macchetto, F. D., Rix, H.-W., & Schneider, D. P. 1996, ApJS, 107, 215
Marcum, P. M., et al. 1997, in The Ultraviolet Universe at Low and High Redshift, ed. W. H. Waller et al. (Woodbury: AIP), 88
Martin, C., et al. 1997, BAAS, 191, 6304
Meurer, G. R., Heckman, T. M., Leitherer, C., Kinney, A., Robert, C., & Garnett, D. R. 1995, AJ, 110, 2665
Mihalas, D., & Binney, J. 1981, Galactic Astronomy (San Francisco: Freeman)
O'Connell, R. W. 1997a, in The Ultraviolet Universe at Low and High Redshift, ed. W. H. Waller et al. (Woodbury: AIP), 11
———. 1997b, in Star Formation Near and Far, ed. S. S. Holt & L. G. Mundy (New York: AIP), 491
———. 1999, ARA&A, 37, 603
O'Connell, R. W., & Marcum, P. M. 1996, in *HST* and the High Redshift Universe, ed. N. R. Tanvir, A. Aragon-Salamanca, & J. V. Wall (Singapore: World Scientific)
Ohl, R. G., et al. 1998, ApJ, 505, L11
Prugniel, P., & Heraudeau, P. 1998, A&AS, 128, 299
Reichen, M., Kaufman, M., Blecha, A., Golay, M., & Huguenin, D. 1994, A&AS, 106, 523
Sandage, A. 1961, The Hubble Atlas of Galaxies (Washington: Carnegie Institution)
Sandage, A., & Brucato, R. 1979, AJ, 84, 472
Smith, A. M., et al. 1997, in The Ultraviolet Universe at Low and High Redshift, ed. W. H. Waller et al. (Woodbury: AIP), 439
———. 2000, ApJ, submitted (preprint astro-ph/0009138)
Smith, D. A., et al. 1996, ApJ, 473, L21
Stecher, T. P., Bohlin, R. C., Hill, J. K., & Jura, M. A. 1982, ApJ, 255, L99
Stecher, T. P., et al. 1997, PASP, 109, 584
Storchi-Bergmann, T., Wilson, A. S., & Baldwin, J. A. 1996, ApJ, 472, 83
Stover, R. J. 1988, in Instrumentation for Ground-Based Optical Astronomy, ed. L. B. Robinson (New York: Springer), 443
Teplitz, H. I., Gardner, J. P., Malumuth, E. M., & Heap, S. R. 1998, ApJ, 507, L17
Tody, D. 1986, Proc. SPIE, 627, 733
Tully, R. B. 1988, Catalog of Nearby Galaxies, (Cambridge: Cambridge Univ. Press)
Waller, W. H., et al. 1995, AJ, 110, 1255
———. 1997a, ApJ, 481, 169
———. 1997b, in The Ultraviolet Universe at Low and High Redshift, ed. W. H. Waller et al. (Woodbury: AIP), 39
———. 1997c, in Star Formation Near and Far, ed. S. S. Holt & L. G. Mundy (New York: AIP), 287
———. 2000, AJ, submitted
Williams, R. E., et al. 1996, AJ, 112, 1335
Witt, A. N., Petersohn, J. K., Bohlin, R. C., O'Connell, R. W., Roberts, M. S., Smith, A. M., & Stecher, T. P. 1992, ApJ, 395, L5
Yi, S., Lee, Y.-W., Woo, J.-H., Park, J.-H., Demarque, P., & Oemler, A. 1999, ApJ, 513, 128